

# Comprehensive proteomic analysis of the main liver and attached liver of *Glyptosternum maculatum* on the basis of data-independent mass spectrometry acquisition

G. Zhang<sup>1,2</sup>, Z. Mou<sup>3</sup>, H. Wang<sup>4,\*</sup> and H. Liu<sup>3,\*</sup>

<sup>1</sup> Anhui Polytechnic University, Academy of Biological and Food Engineering, Department of Food Science and Engineering, 241000 Wuhu, China

<sup>2</sup> Tibet Academy of Agricultural and Animal Husbandry Sciences, Academy of Aquatic Sciences, 850002 Lhasa, China

<sup>3</sup> Tibet Academy of Agricultural and Animal Husbandry Sciences, Institute of Fisheries Science, 850002 Lhasa, China

<sup>4</sup> Hefei Normal University, Academy of Life Science, Department of Biotechnology, 230601 Hefei, China

**KEY WORDS:** attached liver, data independent acquisition, *Glyptosternum maculatum*, main liver, proteomics

Received: 25 April 2022

Revised: 25 August 2022

Accepted: 14 September 2022

\* Corresponding author:

e-mail: wang\_h\_s@126.com; luihappying@163.com

**ABSTRACT.** *Glyptosternum maculatum* Regan is a teleost species endemic to the Brahmaputra River. This species has two livers, namely the attached liver (AL), and the main liver (ML). However, the biological functions and molecular mechanisms of these two livers remain uncharacterised. In this study, we used a comparative quantitative proteomics involving data-independent acquisition to elucidate the functions of ML and AL. A total of 63 differentially expressed proteins (DEPs) were identified. According to the Gene Ontology enrichment analysis, these proteins are involved in cellular processes, metabolic processes, and hydrolase activities. Analysis of the Kyoto Encyclopedia of Genes and Genomes indicated that the enriched pathways among these DEPs were “pancreatic secretion” and “protein digestion and absorption” (i.e., digestive functions). Moreover, 569 highly expressed proteins in both ML and AL were functionally annotated, revealing their diverse biological activities that may involve adaptive responses to cold and hypoxic conditions at high altitudes.

## Introduction

*Glyptosternum maculatum* – a glyptosternoid fish species – inhabits the mid-reaches of the Yarlung Zangbo River and its branches flowing in the Tibetan highlands of China (Xiao et al., 2021). An important characteristic of this fish is the presence of two livers. More specifically, in addition to the main liver (ML), there is another structure called attached liver (AL). The AL, which is located near the base of the pectoral fins between the muscular layer and the skin, is attached to the ML by fusiform tissue (i.e., the joint belt) (Li et al., 2017). Previous research on 11 related species revealed the presence of AL

in five other species in addition to *G. maculatum* (i.e., *Euchiloglanis davidi*, *Pseudecheneis sulcatus*, *Clarias gariepinus*, *Pareuchiloglanis kamengensis*, and *Glarioglanis*). In contrast, other related species (cyprinid and cobitid fishes), which inhabit a similar ecological niche, have only one liver (Li et al., 2021; Zhang et al., 2021). This suggests that the presence of two livers does not provide catfish with an evolutionary advantage (Xiao et al., 2021). Additionally, the histological features and electrophoretogram bands for esterase, alcohol dehydrogenase, malate dehydrogenase, and lactate dehydrogenase isozymes of AL are similar to those of ML. Recent studies have revealed a that portion

of the liver is associated with adaptations to high altitude and cold conditions (Liu et al., 2018; Wong et al., 2021). There is relatively little information available regarding the development of AL and its differentiation during embryogenesis. However, Zhang et al. (2021) have recently reported that AL forms in three stages. In *G. maculatum*, AL does not develop until the larva exits the egg envelope. This is followed by the formation of a visible nodule on approximately day 17, after which a distinct AL is detectable on day 22. These studies have clarified whether AL provides fish with an advantage or if it is simply a basic part of the digestive tract.

Although some studies have been carried out on the histological structures of the liver outside and inside the abdominal cavity, the precise biological functions and potential molecular mechanisms of the two livers in *G. maculatum* are still unclear. Proteomic analysis of any tissue may provide insights into the tissue status and cellular changes under specific conditions (Dietrich et al., 2021; Wang et al., 2021; Wong et al., 2021). Data-independent acquisition (DIA) is a recently developed method involving bioinformatic algorithms and mass spectrometry. In DIA, all tryptic peptide-related fragmentation spectra in each period are captured without any pre-selection of precursor ions, leading to an unbiased examination of multiplexed fragmentation spectra for all peptide precursors in a given tissue (Anjo et al., 2017). Therefore, the unbiased DIA method enables a global, precise, and highly reproducible analysis of ML and AL functions in *G. maculatum*. In the current study, we conducted a DIA-based quantitative proteomic analysis to determine differentially abundant proteins between ML and AL. The generated data were used to functionally characterise the proteins on the basis of the Cluster of Orthologous Groups (COG), Gene Ontology (GO), and Kyoto Encyclopedia of Genes and Genomes (KEGG) databases. Parallel reaction monitoring (PRM) is an emerging high-throughput quantitative approach for the analysis of predefined proteins using high-resolution mass spectrometry (MS) (Zhang et al., 2022). One of the advantages of PRM over conventional antibody-based detection methods (e.g., Western blotting) is the fact that antibodies are not required (Han et al., 2021). Hence, differentially expressed proteins (DEPs) were validated according to PRM to verify the results of DIA-based proteomic analysis. This study may be relevant for the development of a reference proteome dataset useful for the study of liver evolution in catfish.

## Material and methods

### Sample preparation

Adult *G. maculatum* fish ( $n = 60$ ) were collected from the Nyingchi reach (approximately 2800 m above sea level; 29°50'N, 93°25'E) of the Yarlung Zangbo River in Tibet in July 2020. The captured fish were transferred to the Animal Genetics, Breeding and Reproduction Laboratory of the Tibetan Agricultural and Animal Husbandry College and held in an aquarium containing aerated flowing river water. All procedures were conducted in accordance with the “Guiding Principles in the Care and Use of Animals” (China) and were approved by the Laboratory Animal Ethics Committee of the Qinghai University of Medicine Sciences (P20190515-2). Fish were acclimated for 3 days before blood collection. During the acclimation period, water temperature and dissolved oxygen concentration were maintained at  $13 \pm 0.5$  °C and  $8.9 \pm 0.6$  mg/l, respectively (SYXK-2013-100). Examination of 30 randomly selected healthy fish showed that the average length was  $21.43 \pm 2.66$  cm (15.8–28.2 cm) and the average wet weight was  $108.07 \pm 39.73$  g (45.79–232.12 g). Fish livers (AL and ML, three replicates of each sample were selected) were removed and dissected in ice-cold PBS buffer (150 mM NaCl and 2 mM Na<sub>2</sub>HPO<sub>4</sub>; pH adjusted to 8.0 using 0.1 M NaH<sub>2</sub>PO<sub>4</sub>) (Shanghai Bohu Biotechnology Co., LTD, Shanghai, China). Both livers were stored at –80 °C for subsequent quantitative proteomic analysis.

### Protein extraction, protein quantification, and polyacrylamide gel electrophoresis

Proteins were extracted from both livers (ML and AL) as previously described (Wiśniewski et al., 2009). Protein concentrations in the supernatants were determined using bicinchoninic acid kits and the Bradford method (Khramtsov et al., 2021). For sodium dodecyl sulphate polyacrylamide gel electrophoresis (SDS-PAGE) analysis, protein samples were prepared in electrophoresis sample buffer and then heated at 95 °C for 5 min. SDS-PAGE (Shanghai Bohu Biotechnology Co., LTD, Shanghai, China) was carried out using a slab mini-gel apparatus, with a 10% polyacrylamide separating gel and a 4% polyacrylamide stacking gel (Shanghai Bohu Biotechnology Co., LTD, Shanghai, China). An aliquot of each protein sample (20 µl) was added to the gel wells.

## Mass spectrometry data acquisition

From each samples, approx. 150 mg of powder were dissolved in 1 ml of lysis buffer (Tris base pH 8, 8 mol/l CH<sub>4</sub>N<sub>2</sub>O, 1% SDS w/v) and a complete protease inhibitor cocktail (Sigma) was added before homogenisation (Thermo Fisher Scientific, Waltham, MA, USA). The homogenized mixtures were then kept at -20 °C for 20 min and centrifuged for 15 min at 12000 g (4 °C). The top layer was collected in a pre-labelled tube to determine protein purity and concentration using the Bradford method (Thermo Fisher Scientific, Waltham, MA, USA) (Whiffen et al., 2007). Four volumes of 10 mM DTT (in cold acetone, Shanghai Jinli Pharmaceutical Co., Ltd., Shanghai, China) were mixed with the sample extract, vortexed well and incubated at -20 °C for 2 to 12 h. The test materials were centrifuged, precipitate was collected and washed with cold acetone (twice), and subsequently suspended in dissolution buffer (pH 8, 8 mol/l CH<sub>4</sub>N<sub>2</sub>O). Protein samples were diluted in 100 mM triethylammonium bicarbonate (Shanghai Jinli Pharmaceutical Co., Ltd., Shanghai, China) before adding trypsin for an overnight digestion at 37 °C. The resulting peptides were desalted using a Strata-X C18 SPE column (Agilent Technologies, Santa Clara, CA, USA) and then vacuum-dried. The separated peptides were then subjected to sodium/iodide symporter sources. Tandem mass spectrometry (MS/MS) analysis was performed using the Q Exactive™ Plus system (Thermo Fisher Scientific, Waltham, MA, USA) coupled online to an ultra-high performance liquid chromatography (UHPLC) system (Goeminne et al., 2018).

An EASY-nLC™ 1200 UHPLC system (Thermo Fisher Scientific, Waltham, MA, USA) used for shotgun proteomic analysis was connected to an Orbitrap Q Exactive HF-X MS system (Thermo Fisher Scientific, Waltham, MA, USA), which operated in the data-dependent acquisition (DDA) mode. An Acclaim PepMap100 C18 Nano-Trap column (2 cm × 100 µm; 5 µm) (Thermo Fisher Scientific, Waltham, MA, USA) was injected with 2 µg of peptides from fractionated samples, which were reconstituted in 0.1% CH<sub>2</sub>O<sub>2</sub>. Peptides were separated on a Reprosil-Pur 120 C18-AQ analytical column (15 cm × 150 µm, 1.9 µm; Agilent Technologies, Santa Clara, CA, USA) using the following linear gradient over 120 min: 5–100% solvent B (0.1% CH<sub>2</sub>O<sub>2</sub> in 80% ACN) and solvent A (0.1% CH<sub>2</sub>O<sub>2</sub> in ddH<sub>2</sub>O) at a flow rate of 600 nL/min. The mobile phase gradient was as follows: 5–10% B, 2 min; 10–40% B,

105 min; 40–50% B, 5 min; 50–90% B, 3 min; and 90–100% B, 5 min.

A Q Exactive HF-X system (Agilent Technologies, Santa Clara, CA, USA) was operated in positive polarity mode with a spray voltage of 2.3 kV and a capillary temperature of 320 °C. Full MS scans (350–1500 m/z) were developed at a resolution of 60000 (at 200 m/z), with an automatic gain control (AGC) mark value of  $3 \times 10^6$  and an ion injection time of 20 ms. Based on the full MS scans, 40 most abundant precursor ions were used for higher energy collisional dissociation fragment analysis at a resolution of 15000 (at 200 m/z) with an AGC mark value of  $1 \times 10^5$ , an ion injection time of up to 45 ms, a normalised collision energy of 27%, an intensity threshold of  $8.3 \times 10^3$ , and a dynamic exclusion parameter of 60 s.

For DIA experiments, each sample was reconstituted in 0.1% CH<sub>2</sub>O<sub>2</sub>, mixed with 0.2 µL standard peptides (iRT kit; Biognosys, Thermo Fisher Scientific, Waltham, MA, USA), and injected into an EASY-nLC™ 1200 UHPLC system (Thermo Fisher Scientific, Waltham, MA, USA) coupled to an Orbitrap Q Exactive HF-X MS system (Thermo Fisher Scientific, Waltham, MA, USA) operating in DIA mode. The applied liquid conditions were the same as described above. For DIA, the MS1 and MS2 resolutions were fixed at 60000 and 30000 (200 m/z), respectively. The m/z range was 350–1500 for variable 30 cycles. The full scan of AGC targets were set at  $3 \times 10^6$  and IT was set at 50 ms. DIA settings were as follows: NCE, 27%; target value,  $1 \times 10^6$ ; and maximum injection time, auto (to allow the MS system to continuously operate in the equivalent ion addition and detection mode). Details regarding the 30 cycles are provided in Table 1.

PRM experiments were completed using a fused-silica microcolumn (20 cm) (Thermo Fisher Scientific, Waltham, MA, USA) and a 1-h linear gradient at the optimum temperature for peptide isolation. Liquid chromatography and MS programs were as described for shotgun proteomics and DIA experiments. A “sensitive” method was implemented for this analysis, as previously described (Kelstrup et al., 2012). Full MS survey and PRM transitions were acquired at a resolution of 35000. The PRM isolation width was 1.6 Da, AGC was set to  $2 \times 10^5$ , and the maximum number of iterations was set to auto. All spectra were recorded in the profile mode. Data for the AL and ML samples were collected using DIA and DDA modes. All liver samples were used for PRM data acquisition.

**Table 1.** Details of 30 cycles of data-independent acquisition experiments

Width, Da	Start, Da	End, Da	Median, Da
25	350	375	362.5
22	375	397	386.0
18	397	415	406.0
18	415	433	424.0
18	433	451	442.0
18	451	469	460.0
18	469	487	478.0
18	487	505	496.0
18	505	523	514.0
18	523	541	532.0
18	541	559	550.0
18	559	577	568.0
18	577	595	586.0
18	595	613	604.0
20	613	633	623.0
20	633	653	643.0
20	653	673	663.0
25	673	698	685.5
25	698	723	710.5
25	723	748	735.5
25	748	773	760.5
25	773	798	785.5
25	798	823	810.5
32	823	855	839.0
32	855	887	871.0
45	887	932	909.5
53	932	985	958.5
62	985	1047	1016.0
97	1047	1144	1095.5
339	1144	1483	1313.5

## Mass spectrometry data analysis

DDA and DIA MS data were analysed using Proteome Discoverer 2.2 (Thermo Fisher Scientific, Waltham, MA, USA), Biognosys Spectronaut (version 9.0), and the R software. DDA MS data were analysed using PD 2.2 and applied for the protein database search [XZ\_fish\_pasa2.longest.pep.filter.fasta (24489 sequences)] (<https://doi.org/10.1111/jfb.14877>) (Zhang et al., 2021). N-terminal acetylation and methionine oxidation were set as flexible modifications and cysteine carbamidomethylation was set as a fixed modification. The false detection rate, determined by reverse database analysis, was set at 5% for proteins and peptides. Enzyme specificity was set to trypsin (enabling cleavage before proline), and a maximum of two missed cleavages were allowed in the database search. To characterise peptides, an initial precursor mass deviation of up to 10 ppm was permitted, as was a fragment mass deviation of 10 ppm. Label-free quantification based on

MS1 was performed using the maxLFQ algorithm as previously described (Qi et al., 2021).

GO analysis was conducted using the InterProScan 5 software and non-redundant protein databases (e.g., Pfam, PRINTS, ProDom, SMART, ProSiteProfiles, and PANTHER) (Kelstrup et al., 2017). The COG (Bruderer et al., 2015) and KEGG databases were used to analyse protein families and pathways (Liao et al., 2022). An enrichment pipeline (Shao et al., 2014) was used for GO and KEGG enrichment analyses. The results of PD 2.2 analysis of the DDA data were applied to construct a spectral library. To confirm that peptide identities and quantities were accurate, the imported PRM data spectrum was compared with that of the spectral library. The mProphet algorithm was used to confirm that peak selection and peak integration were appropriate. Moreover, the chromatograms of the nominated fragments of total extracted ions were reviewed.

## Results

### Data-independent acquisition workflow and protein identification

ML and AL positions within the body of *G. maculatum* are presented in Figure 1. Proteins in ML and AL tissues were extracted, purified, and digested to generate the peptide spectral library. The Q Exactive HF-X system (Kelstrup et al., 2017) in DDA mode was used for shotgun proteomic analysis of individual samples (Figure 2A). To classify peptides and proteins, PD 2.2 was used to analyse the DDA MS data. The spectral library was constructed based on the PD 2.2 search results using Spectronaut (version 9). The final spectral library contained peptides

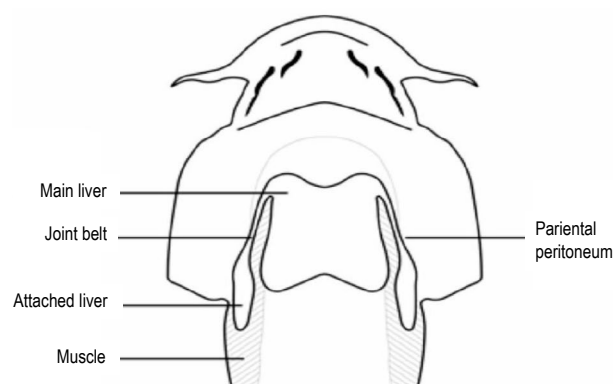


**Figure 1.** Sketch of *Glyptosternum maculatum* liver divided into two parts, one placed outside the abdominal cavity representing the attached liver in green oval shape, connected to another portion located inside the cavity representing the main liver. Image obtained from Huijuan Z. (2011)

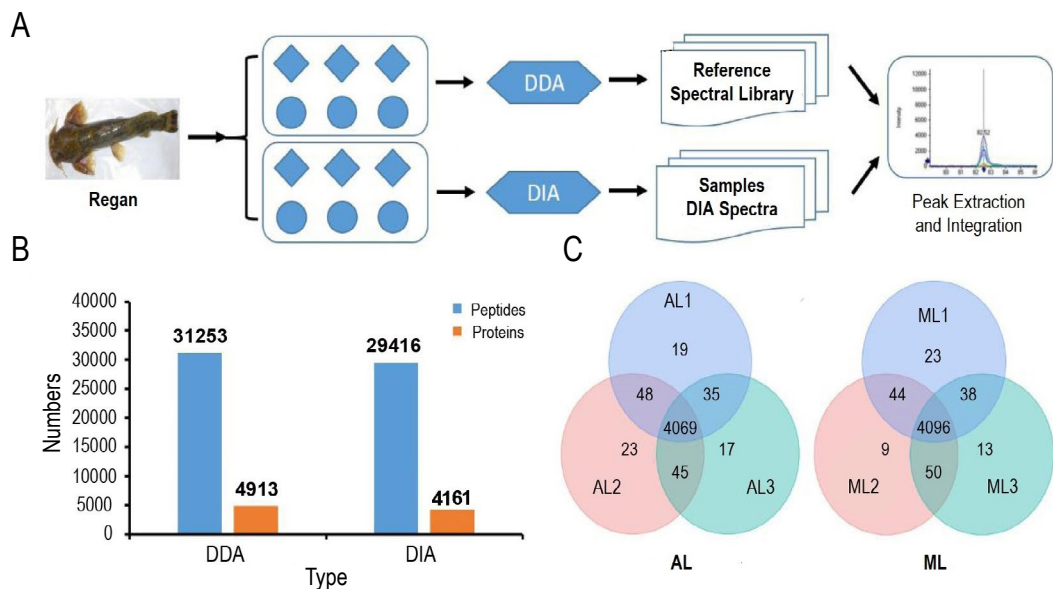


**Figure 2.** Proteome analysis of the main and attached liver of *Glyptosternum maculatum* A) workflow of DIA proteomic quantification; circle indicates the main liver (ML) and square indicates the attached liver (AL). Q-Exactive HF mass spectrometry was used for data-dependent acquisition (DDA) and data-independent acquisition (DIA). Peak extraction and integration was performed in Spectronaut; B) quantitative results of DDA and DIA; C) analytical replicates. Venn diagram showing individual replicates of quantified proteins. Over 95% of proteins were determined in all replicates ( $n = 3$ )

and proteins that were selected using the false discovery rate threshold of 1%. The DIA MS data for all six runs were analysed using Spectronaut based on the spectral library obtained for the DDA MS data. DDA data analysis resulted in the identification of 31253 peptides and 4913 proteins (Figure 2B), whereas DIA data analysis identified 29416 peptides and 4161 proteins (Figure 2B) (i.e. 94.1 and 87.2% of peptides and proteins identified from the DDA MS data, respectively). Moreover, the results for triplicate ML and AL samples indicated that the DIA pipeline was highly reproducible, with approximately 95% of the proteins quantified (Figure 2C).

### Analysis of proteome-level differences between AL and ML and identification of highly expressed proteins

A hierarchical cluster heat map ( $\log_2$  scale) was plotted according to the expression ratios of proteins identified in ML and AL. The overall regulatory patterns were similar between AL and ML (Figure 3A), with some major differences in individual proteins. Protein IDs, gene symbols, and relative protein ratios for the 4161 identified proteins are listed in Table S1. A volcano plot was constructed for DEPs according to geometric means of the expression ratios and combined  $P$ -values (Student's  $t$ -test) for the 4161 identified proteins. For DEP analysis, fold-change in protein expression was calculated as the ratio of the mean value to the value of all biological replicates for each protein in a pairwise compari-

son. Selected proteins were further screened to detect significant changes in protein expression (i.e., fold-change  $< 0.667$  or  $> 1.5$  and  $P < 0.05$ ). Finally, 63 significant DEPs were identified, of which 48 and 15 were more and less abundant in ML than in AL, respectively (Figure 3B and Table 2).

Fifteen unique proteins were identified in AL, among which the most abundant were cytoplasmic dynein 1 light intermediate chain 1, peroxisomal membrane protein 4 (PXMP4), ubiquitin-associated protein 2, Rho guanine nucleotide exchange factor 1 (ARHG1), AMP deaminase 1, WD repeat domain phosphoinositide-interacting protein 3 (WIPI3), and probable 18S rRNA methyltransferase protein 1. In contrast, the most abundant proteins in ML were calpain-7, periostin, insulin, keratin, type 1 cytoskeletal 13, protein PRRC2C, Bcl-2-like protein 1 (B2CL1), nidogen-1, NEDD8-activating enzyme E1 catalytic subunit (UBA3), MARCKS-related protein, chymotrypsin-like elastase family member 2A (CEL2A\_2), lysozyme g, major facilitator superfamily protein 12, Bcl 10-interacting CARD protein, epithelial cell adhesion molecule, UPF0449 protein C 19orf25 homolog, E3 ubiquitin-protein ligase NEURL3, homeobox protein cut-like 1, putative hexokinase, conserved oligomeric Golgi complex subunit 8, and unidentified enm.model.chr 19.80 (-).

The hierarchical clustering of DEPs into two groups suggested that AL may have arisen due to large changes in protein levels during evolution.

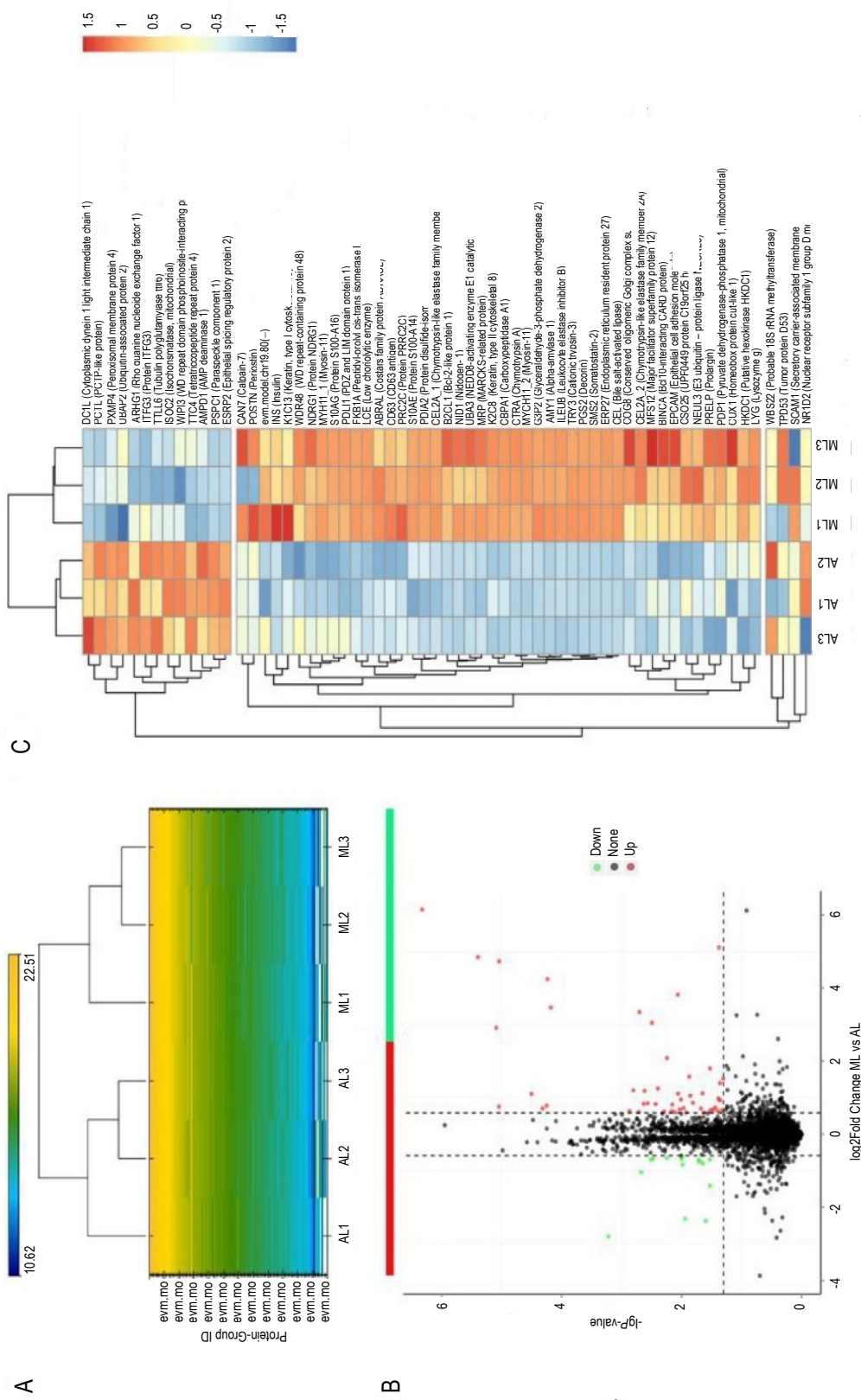


**Figure 3.** Analysis of proteome changes between the main and attached liver. **A)** distribution of 4282 proteins was clustered based on the expression ratio (log<sub>2</sub> scale); each row in the coloured heat map represents individual proteins; **B)** volcano plots of the complete set of 4282 proteins (commonly identified in 3 experiments); each data point represents expression level of individual proteins (X axis: log<sub>2</sub> fold change value) and their corresponding P-values (Y axis: -log<sub>10</sub> of t-test's); black dashed lines represent the threshold for differential expression (cut-off = 1.5-fold and P-value ≤ 0.05). Solid red and green dots indicate significantly increased and decreased expression of proteins, respectively; **C)** heatmap showing the expression profiles and hierarchical clustering of 63 differentially expressed proteins (experiments were performed in triplicates); AL – attached liver; ML – main liver

**Table S1.** Final list of identified proteins in the main liver (ML) and attached liver (AL) (differentially expressed proteins)

Protein	ML-1	ML-2	ML-3	AL-1	AL-2	AL-3	ML vs AL FC	ML vs AL P-value	ML vs AL log <sub>2</sub> FC	Signifi- cant
evm.model.chr4.379	12794.80	14292.51	13327.89	20066.21	20946.86	24655.05	0.62	0.02	-0.70	Down
evm.model.chr7.1233	55819.81	66434.43	57747.10	88706.57	101943.24	101500.52	0.62	0.00	-0.70	Down
evm.model.chr1.1052	3104.34	4833.57	4507.63	6953.25	7404.48	7320.94	0.57	0.02	-0.80	Down
evm.model.chr24.285	0.00	8749.51	10589.29	14557.17	17950.12	16141.73	0.60	0.02	-0.75	Down
evm.model.chr21.425	40619.74	3508.64	13475.63	111231.11	69942.70	104420.08	0.20	0.01	-2.31	Down
evm.model.chr10.1256	200926.48	4021.36	8913.82	296933.50	420042.53	389997.91	0.19	0.03	-2.37	Down
evm.model.chr2.373	19300.21	15085.29	18249.65	23831.87	28073.74	28655.26	0.65	0.01	-0.61	Down
evm.model.chr10.808.3	106261.12	82965.45	96292.96	159926.81	154759.17	140745.39	0.63	0.00	-0.67	Down
evm.model.chr2.233	5038.57	3308.77	5490.60	8024.71	7965.96	6461.07	0.62	0.03	-0.70	Down
evm.model.chr7.1014	4931.09	5337.60	6589.78	8976.36	8567.59	9409.83	0.63	0.01	-0.68	Down
evm.model.chr14.697	38230.94	42511.78	47448.48	67455.22	72548.98	60891.96	0.64	0.01	-0.65	Down
evm.model.chr12.172	86511.35	90291.34	85826.85	183509.44	186598.52	169011.59	0.49	0.00	-1.04	Down
evm.model.chr15.299.2	8221.66	13405.32	11654.05	83708.05	74056.56	73137.02	0.14	0.00	-2.79	Down
evm.model.chr11.1013.3	3733.16	17205.64	15559.05	0.00	35163.46	29375.03	0.38	0.03	-1.41	Down
evm.model.chr9.471	4848.29	6999.20	6949.76	11544.15	10787.60	0.00	0.56	0.01	-0.83	Down
evm.model.chr10.298	46952.89	0.00	53078.84	16240.23	17489.71	18636.15	2.87	0.05	1.52	UP
evm.model.chr19.80	29613.81	26163.05	23452.61	8832.36	12638.34	20154.16	1.90	0.04	0.93	UP
evm.model.chr22.74	867868.50	472762.56	503758.94	0.00	26399.69	9248.54	34.49	0.04	5.11	UP
evm.model.chr7.1349	157914.70	129705.69	115436.77	91559.72	70525.58	96518.34	1.56	0.04	0.64	UP
evm.model.chr2.1232	20286.59	24155.07	25651.53	8367.43	2736.41	15551.37	2.63	0.04	1.39	UP
evm.model.chr4.230	15638.28	14887.13	17294.35	8473.97	7849.08	10661.49	1.77	0.00	0.83	UP
evm.model.Contig293_pilon.5	30245.71	29061.01	30304.25	19228.17	17226.61	23118.25	1.50	0.02	0.59	UP
evm.model.chr11.1241	123721.84	125256.46	127277.25	73418.02	67025.94	96288.80	1.59	0.03	0.67	UP
evm.model.chr6.1003	71790.41	73810.91	75334.61	41734.12	42115.93	57105.14	1.57	0.03	0.65	UP
evm.model.chr24.268	786324.06	776343.56	774007.69	472929.44	487827.53	552546.50	1.54	0.01	0.63	UP
evm.model.chr6.584	825445.00	848662.44	833270.31	136910.19	11444.43	155608.53	8.25	0.00	3.04	UP
evm.model.chr2.1086	21017.68	21386.29	18456.53	12300.32	9280.34	12221.55	1.80	0.00	0.85	UP
evm.model.chr2.708	88755.69	83050.88	79349.74	52527.02	39503.48	48966.04	1.78	0.00	0.83	UP
evm.model.chr4.871	25260.98	21561.67	19749.03	10060.53	6810.78	11090.38	2.38	0.00	1.25	UP
evm.model.chr16.771	258391.34	253688.89	252756.38	148941.75	179941.67	178817.70	1.51	0.01	0.59	UP
evm.model.chr1.167	185736.72	192565.63	186385.22	21995.94	63445.07	47700.87	4.24	0.01	2.08	UP
evm.model.chr24.474	339086.75	327197.88	324168.00	119581.80	154124.58	156868.86	2.30	0.00	1.20	UP
evm.model.chr18.702	92384.68	92465.88	105159.97	57545.68	59948.05	59209.20	1.64	0.01	0.71	UP
evm.model.chr16.411	32397.81	29793.60	34110.12	20314.89	20232.65	19668.07	1.60	0.01	0.68	UP
evm.model.chr18.723	118205.34	110405.43	126943.44	74515.16	79680.46	79543.89	1.52	0.01	0.61	UP
evm.model.chr9.532	34885.48	32573.86	36237.97	20985.25	22504.92	23331.09	1.55	0.00	0.63	UP
evm.model.chr18.831	86235.58	85566.52	90903.13	46395.47	34185.23	34663.85	2.28	0.00	1.19	UP
evm.model.chr7.594	191163.16	195681.33	196586.95	37084.84	9160.22	11253.57	10.15	0.00	3.34	UP
evm.model.chr3.589	593136.19	624286.19	654094.75	38083.64	72457.99	59266.98	11.02	0.00	3.46	UP
evm.model.Contig293_pilon.6	240462.53	228996.97	224879.28	214002.63	211553.17	204741.53	1.10	0.03	0.14	UP
evm.model.Contig70_pilon.42	429518.53	410615.56	414195.81	244657.36	248036.91	235816.31	1.72	0.00	0.78	UP
evm.model.chr3.21	139338.89	130218.77	134837.03	9934.33	2583.03	1556.06	28.73	0.00	4.84	UP
evm.model.chr4.1200	65952.91	63298.23	65994.68	31817.79	31147.07	28054.76	2.15	0.00	1.10	UP
evm.model.chr6.1432	254397.95	249773.27	238291.14	15318.35	10820.27	0.00	18.94	0.00	4.24	UP
evm.model.chr14.161	536741.00	529914.88	525141.50	327826.38	325257.66	323439.00	1.63	0.00	0.70	UP
evm.model.chr3.165	3451054.75	3375108.75	3312039.00	123586.22	5578.23	13865.32	70.88	0.00	6.15	UP
evm.model.chr1.325	431316.56	425267.53	434226.31	19783.27	5678.35	23279.04	26.48	0.00	4.73	UP
evm.model.chr11.1356	299633.63	289384.75	285895.69	40178.42	28235.24	47566.04	7.54	0.00	2.92	UP
evm.model.chr13.536	7588.54	9758.29	11229.93	4350.32	4948.37	5218.00	1.97	0.04	0.98	UP
evm.model.chr24.474	339086.75	327197.88	324168.00	119581.80	154124.58	156868.86	2.30	0.00	1.20	UP
evm.model.chr13.554.1	746.29	827.81	1032.12	635.28	525.73	499.27	1.57	0.05	0.65	UP
evm.model.chr19.718	13542.77	13943.41	17364.19	9550.32	6004.92	9147.01	1.82	0.02	0.86	UP

continued on the next page

**Table S1.** continued

Protein	ML-1	ML-2	ML-3	AL-1	AL-2	AL-3	ML vs AL FC	ML vs AL P-value	ML vs AL $\log_2$ FC	Signifi- cant
evm.model.chr6.1363	14795.34	17864.92	24626.85	4197.17	0.00	6780.51	3.48	0.03	1.80	UP
evm.model.chr12.1101	90621.37	110225.27	95840.31	67377.67	33140.45	36196.64	2.17	0.02	1.12	UP
evm.model.chr24.295	808126.06	896903.75	811631.06	597837.25	505484.81	549001.38	1.52	0.00	0.61	UP
evm.model.chr19.567	58264.28	56873.97	62984.36	41151.78	41473.11	33056.03	1.54	0.01	0.62	UP
evm.model.chr21.163	56109.70	63218.16	70878.59	41235.67	29967.83	20510.54	2.07	0.01	1.05	UP
evm.model.chr11.1018	5117.28	5232.21	6788.70	2485.06	4056.83	3804.86	1.66	0.04	0.73	UP
evm.model.chr6.696	21576.60	23096.17	21028.71	12084.63	13404.73	8488.85	1.93	0.01	0.95	UP
evm.model.chr7.988	37097.28	44012.22	42937.25	22569.46	32008.71	21735.81	1.63	0.02	0.70	UP
evm.model.chr4.1045.1	0.00	49865.04	50586.73	0.00	24160.11	22370.43	2.16	0.01	1.11	UP
evm.model.chr12.715	8804.51	9540.16	0.00	5915.67	4625.94	5135.59	1.76	0.01	0.81	UP
evm.model.chr5.211	26026.98	0.00	22887.56	6760.87	10412.65	7421.29	2.98	0.01	1.58	UP

**Table 2.** Differentially expressed proteins between the main liver (ML) and attached liver (AL) in *Glyptosternum maculatum*

(a) – Protein with relatively high abundance specific for the AL

	Protein name	Abundance in ML	Abundance in AL	$\log_2$ FC	P-value
1	DC1L1 (Cytoplasmic dynein 1 light intermediate chain 1)	-	+	-0.700295	0.019279
2	PCTL (PCTP-like protein)	-	+	-0.698703	0.003050
3	PXMP4 (Peroxisomal membrane protein 4)	-	+	-0.800648	0.022576
4	UBAP2 (Ubiquitin-associated protein 2)	-	+	-0.745950	0.019810
5	ARHG1 (Rho guanine nucleotide exchange factor 1)	-	+	-2.309724	0.011395
6	ITFG3 (Protein ITFG3)	-	+	-2.371871	0.025336
7	TTLL6 (Tubulin polyglutamylase ttll6)	-	+	-0.614053	0.010027
8	ISOC2 (Isochorismatase, mitochondrial)	-	+	-0.673644	0.003347
9	WIPI3 (WD repeat domain phosphoinositide-interacting protein 3)	-	+	-0.698197	0.029523
10	TTC4 (Tetratricopeptide repeat protein 4)	-	+	-0.677013	0.009941
11	AMPD1 (AMP deaminase 4)	-	+	-0.648153	0.005693
12	PSPC1 (Paraspeckle component 1)	-	+	-1.037576	0.002111
13	ESRP2 (Epithelial splicing regulatory protein 2)	-	+	-2.794506	0.000605
14	WBS22 (Probablr 18s rRNA methyltransferase protein 1)	-	+	-1.407310	0.029703
15	NR1D2 (Nuclear receptor subfamily 1 group D member 2)	-	+	-0.833538	0.010354

(b) – Proteins of relatively high abundance in ML

16	CAN7 (Calpain-7)	+	-	1.518715	0.049183
17	enm.model.chr 19.80 (-)	+	-	0.928591	0.043685
18	INS (Insulin)	+	-	0.591076	0.041751
19	K1C13 (Keratin, type 1 cytoskeletal 13)	+	-	0.640241	0.039664
20	WDR48 (WD repeat-containing protein 48)	+	-	1.394857	0.043519
21	NDRG1 (Protein NDRG1)	+	-	0.825474	0.003700
22	MYH11_1(Myosin-11)	+	-	0.589016	0.023669
23	S10AG (Protein S100-A16)	+	-	0.668453	0.033124
24	PDLI1 (PDZ and LIM domain protein 1)	+	-	0.648391	0.030039
25	FKB1A (Peptidyl-prolyl cis-trans isomerase FKB1A)	+	-	0.626756	0.006785
26	LCE (Low choriolytic enzymes)	+	-	3.044211	0.003187
27	ABRAL (Costars family protein ABRACL)	+	-	0.848388	0.002701
28	CD63 (CD63 antigen)	+	-	0.832926	0.002317
29	PRC2C (Protein PRRC2C)	+	-	1.251457	0.004023
30	S10AE (Protein S100-A14)	+	-	0.591172	0.011884
31	PDIA2 (Protein disulfide-isomerase A2)	+	-	2.084488	0.00570
32	CEL2A_1 (Chymotrypsin-like elastase family member 2A)	+	-	0.822806	0.036542
33	B2CL1 (Bcl-2-like protein 1)	+	-	0.714779	0.010742

continue on the next page

**Table 2.** continued

	Protein name	Abundance in ML	Abundance in AL	$\log_2 FC$	P-value
34	NID1 (Nidogen-1)	+	-	0.677421	0.009293
35	UBA3 (NED8-activating enzyme E1 catalytic subunit)	+	-	0.605167	0.007653
36	MRP (MARCKS-related protein)	+	-	0.633999	0.001352
37	K2C8 (Keratin, type II cytoskeletal 8)	+	-	0.776229	0.002406
38	CBPA1 (Carboxypeptidase A1)	+	-	3.342963	0.001966
39	CTRA (Chymotrypsin A)	+	-	3.462227	0.000065
40	MYH11_2 (Myosin-11)	+	-	0.139607	0.025123
41	G3P2 (Glyceraldehyde-3-phosphate dehydrogenase 2)	+	-	0.783895	0.000056
42	AMY1 (Alpha-amylase 1)	+	-	4.844719	0.000004
43	ILEUB (Leukocyte elastase inhibitor B)	+	-	1.101042	0.000031
44	TRY3 (Cationic trypsin-3)	+	-	4.243100	0.000058
45	PGS2 (Decorin)	+	-	0.704931	0.000048
46	SMS2 (Somatostatin-2)	+	-	6.147342	0.0000005
47	ERP27 (Endoplasmic reticulum resident protein 27)	+	-	4.727008	0.000009
48	CEL (Bile salt-activated lipase)	+	-	2.915269	0.000008
49	COG8 (Conserved oligomeric Golgi complex subunit 8)	+	-	0.977129	0.040831
50	CEL2A_2 (Chymotrypsin-like elastase family member 2A)	+	-	1.201823	0.001562
51	MFS12 (Major facilitator superfamily protein 12)	+	-	0.650539	0.046795
52	BINCA (Bcl 10-interacting CARD protein)	+	-	0.860477	0.015443
53	EPCAM (Epithelial cell adhesion molecule)	+	-	1.798675	0.029684
54	CSO25 (UPF0449 protein C 19orf25 homolog)	+	-	1.117772	0.022257
55	NEUL3 (E3 ubiquitin-protein ligase NEURL3)	+	-	0.607015	0.001916
56	PRELP (Prolargin)	+	-	0.622720	0.005095
57	PDP1 (Pyruvate dehydrogenase-phosphatase 1, mitochondrial)	+	-	1.052352	0.013982
58	CUX1 (Homeobox protein cut-like 1)	+	-	0.728036	0.036179
59	HKDC1 (Putative hexokinase HKDC1)	+	-	0.951316	0.009745
60	LYG (Lysozyme g)	+	-	0.700865	0.020908
61	TPD53 (Tumor protein D53)	+	-	1.110253	0.008689
62	SCAM1 (Secretory carrier-associated membrane protein 1)	+	-	0.811656	0.006957
63	POSTN (Periostin)	+	-	1.576872	0.013363

NB(+) signifies high abundance while (-) stands for low abundance and (/) represents un-obtained FC/P-value ( $P < 0.05$  mean that data is significantly different)

Such evolutionary links have been previously studied in six catfish species on the basis of distinct liver transcriptome profiles (Ma et al., 2016). Approximately 13 unique genes in *G. maculatum* have been identified as those associated with the survival under hypoxic conditions at high altitudes. Although this study did not comprehensively determine the differences in ML and AL function, the results presented herein provide insights into the proteins in both livers associated with the ability of *G. maculatum* to adapt to environmental conditions. Secretion-related DEPs, such as PXMP4, were expressed at high levels in AL, indicating a possible role associated with adaptive responses to cold stress. Additionally, Rho GTPase was moderately expressed in AL and may be associated with proteins encoded by rapidly evolving genes identified in an earlier transcriptomic analysis of catfish. Other proteins were mainly related to oxidative activity and energy metabolism, including acyl-CoA dehydrogenase, ATPase, and GTPase (Ma et al., 2016). The unknown proteins identified in

the current study were characterised according to the BLAST analysis of the UniProt database (Figure 3C).

Peng and Wang (2020) have reported that proteins with comparable expression profiles may have similar biological functions. Another study have found that proteins expressed at high levels in the liver may be important for adaptations to high altitudes (Provost et al., 2013). We have identified 569 proteins that were highly expressed in both ML and AL (Table S2). The expression levels of these proteins were significantly higher than the mean expression levels of all proteins in AL and ML ( $P < 0.05$ ).

### Functional classification of differentially expressed and highly expressed proteins

To elucidate the functional differences between ML and AL, 63 DEPs were clustered into 15 functional categories of the COG database (Zhou et al., 2020) (Figure 4A). The major differences between ML and AL were related to post-translational modifications,

**Table S2.** Highly expressed proteins in the attached liver (AL) and main liver (ML)

Protein	ML-1	ML-2	ML-3	AL-1	AL-2	AL-3	ML vs ML log <sub>2</sub> FC
evm.model.chr11.677	604504.125	468838.9375	668734.6875	655188.8125	673835.5625	483933.8125	-0.057536639
evm.model.chr22.604.1	502240.4063	557545.8125	612013.0625	604720.4375	650782.375	633933.4375	-0.176554197
evm.model.chr7.741	557264.125	585778	587410.875	594611.8125	616638.1875	625577	-0.086065996
evm.model.chr2.949	567167.5	563862.6875	581119.8125	624807.75	640452.1875	609469.0625	-0.130872962
evm.model.chr2.467	509345.4063	541560.0625	528730.5625	664163	665039.25	679356.625	-0.346568569
evm.model.chr24.391	601385.5	609157.8125	599342	595207.8125	601466.1875	586693.9375	0.021293896
evm.model.chr3.418	583819.5	622247.8125	629839.625	566217.875	591299.625	604647.25	0.059144118
evm.model.chr12.1145	608681.875	635720.6875	648887.375	566692.8125	567323.125	572480.75	0.149857748
evm.model.chr1.849	618936.625	625417.5625	630643.0625	584642.375	591980	589771.125	0.086081711
evm.model.chr17.403	644732.4375	636370.6875	640195.375	585394.375	576968.125	559372.1875	0.158218833
evm.model.chr3.956	626841.0625	606658.125	615917.3125	597911.375	613031.0625	602778	0.028118066
evm.model.chr21.43	591041.125	585848.5	603505.125	629485.75	635393.4375	621400.25	-0.083346264
evm.model.chr2.768	576409.375	587800.3125	592560.8125	631658.375	643656.5	640194.625	-0.124802447
evm.model.chr17.177	577384.4375	634363.875	630313	560316.125	635918.25	636609.6875	0.007237035
evm.model.chr8.809	609802.9375	572386.4375	594042.875	659829.4375	632577	608887.5	-0.098161355
evm.model.chr15.729	593630.25	615736.9375	623566.9375	603854.5	621950.9375	627512.125	-0.015955169
evm.model.chr21.118	627750.4375	626097.0625	631865.125	570246.25	614749.4375	620777.25	0.062493336
evm.model.Contig940_pilon.14	598357.625	614237.875	603321.25	605246.5	631509.375	642270.4375	-0.049287205
evm.model.chr6.982	625143.75	599363.3125	601692.375	638035.1875	619029.125	623505	-0.042325152
evm.model.chr16.443	518916.2188	531057.875	531604.5	725495.6875	708973.6875	713671.5	-0.441723358
evm.model.chr18.314	642226.5	630444.625	639315.25	609005.5	607230.625	613391.9375	0.063521844
evm.model.chr18.556	631911.1875	618073.75	638685.25	596451	625828.875	661041.75	0.004091393
evm.model.chr1.989	624662.125	634056.125	641348.3125	640128.8125	631814	622952.4375	0.003931861
evm.model.chr16.214	657927.0625	653887.25	652332.875	629307.3125	599788.25	601748.75	0.10139393
evm.model.chr1.1063	629863	646884.375	662006.375	609586.9375	644215.125	609195	0.057504172
evm.model.chr4.591	639982.9375	613654.4375	620170.3125	646805.375	644328	642265.5625	-0.04516646
evm.model.chr1.634	643315.8125	589402.25	584510.125	677380.125	638130.25	684290.625	-0.138116856
evm.model.chr21.408	657520.1875	609996.8125	618537.9375	652381.625	623668.3125	673835.3125	-0.048017525
evm.model.chr18.91	402733.9375	893649.375	958569.75	342431.9375	344501.5	896676.4375	0.509880435
evm.model.chr24.268	786324.0625	776343.5625	774007.6875	472929.4375	487827.5313	552546.5	0.626755956
evm.model.chr11.675	643995.6875	721053.125	715110.3125	507920.4063	660834.5625	611376.375	0.224710202
evm.model.chr12.105	606901.75	574291	605544.8125	706582.75	695951.3125	671887.875	-0.215381623
evm.model.chr16.183	662428.25	662747.5625	664267.375	634633.5	647834.25	618105.375	0.065930166
evm.model.chr15.656	640030.5625	636601.125	667512.5	652277	650321.3125	644320.375	-0.002057411
evm.model.chr6.959	675391.3125	664747.875	662922	646205.375	631222.75	618341.625	0.079422739
evm.model.chr8.438	646191.5	642357.75	649948.4375	681246.0625	655122.6875	639821	-0.027782464
evm.model.chr1.1046	739938.0625	807441	769780.1875	559154.625	518367.0625	521355.8125	0.53529779
evm.model.Contig1133_pilon.4	659916.1875	664293.625	662837.9375	628934.25	660794.5	651410.875	0.033722648
evm.model.Contig1037_pilon.1	663735.5	635161.4375	631903.125	649738.5	675843.25	679391.625	-0.0543843
evm.model.chr2.945	610723.625	633167	644277.1875	682160.5	685641.3125	680756.9375	-0.117622277
evm.model.chr13.139	689947.6875	697220.5625	691151.1875	606418.4375	625084.875	628900.75	0.159801418
evm.model.chr3.259	667363.375	671331	626001.875	672408.25	658544.75	644634.75	-0.007975645
evm.model.chr11.80	644195.125	656768.25	607085.9375	695171.5625	680427.625	690553.8125	-0.114848633
evm.model.chr7.914	669687.125	679653.6875	657687.25	636239.5	663334.9375	671592.875	0.026010551
evm.model.chr18.122	697836.3125	691767.1875	704634.875	646631.0625	615545.9375	623645	0.151232157
evm.model.chr12.789	675782.125	645658.1875	681079.1875	667327.3125	642668.75	672420	0.014556509
evm.model.chr11.704	649705.75	656931.9375	640266.875	680719.6875	683398.5625	674005.5	-0.066059486
evm.model.chr23.390.2	689944.875	695645.1875	678180.125	627672.125	635528.5	661747.75	0.100462573
evm.model.chr18.678	698531.4375	673434.8125	702901.5	652567.9375	653716.0625	632174.5	0.098109534
evm.model.chr3.1300	682146.125	663904.375	677203.75	689477.5625	663162.0625	639702.0625	0.022212534
evm.model.chr9.729	866287.75	64351.72656	68047.71094	1046847.688	1005081.375	994052.4375	-1.608802412

continue on the next page

**Table S2.** continued

Protein	ML-1	ML-2	ML-3	AL-1	AL-2	AL-3	ML vs ML $\log_2$ FC
evm.model.chr20.48	667787.6875	662860.8125	668388.875	685727.1875	694301.5625	687391.3125	-0.048526102
evm.model.chr22.595	690450.4375	669106.6875	663954.125	684641.125	677241.3125	694249.25	-0.023071797
evm.model.chr6.158	681096.625	661548.125	677067.5625	678983.1875	701245.1875	686929.125	-0.033498504
evm.model.chr10.820	704609	682408.125	697513.875	651582.1875	673012.625	681753.3125	0.055150875
evm.model.chr17.855	652305	739781.9375	721090.25	641680.625	656086.5625	700324.3125	0.08079109
evm.model.chr12.327	705211.625	695959.125	704935.875	675831.875	666550.875	675372.0625	0.061827601
evm.model.chr11.1317	660298.4375	636531.375	617089.3125	710405.625	751747.0625	753814.125	-0.211406407
evm.model.chr19.164	726190.6875	684617.75	682672	698928.6875	656071.375	687060.125	0.035878048
evm.model.chr1.321	666531.5	681384.625	669961.1875	705402.1875	705528.625	707148.25	-0.069917982
evm.model.Contig310_pilon.24	664029.5	656639.75	685852.625	717407.8125	716071.375	706322.4375	-0.09278017
evm.model.chr24.295	808126.0625	896903.75	811631.0625	597837.25	505484.8125	549001.375	0.607014706
evm.model.chr21.555	701834.0625	724514.75	739030.4375	703398.3125	693448.25	674978	0.06371788
evm.model.chr9.973	715283.0625	692468.125	718495.1875	707451.3125	740335.25	668308.4375	0.006904379
evm.model.chr20.562	716638.25	740321.4375	719684.4375	700065.125	685248.0625	684208.9375	0.072807878
evm.model.chr22.176	691924.125	672820.5	662759	752528.6875	752281.375	717224.375	-0.132176682
evm.model.chr4.1221	672556.5	696720.125	697738.8125	715096	743920.8125	733520.75	-0.085052396
evm.model.chr19.314	699740.125	705660.875	716180.875	752336.1875	680546.25	723949.9375	-0.023773702
evm.model.chr15.111	722408.9375	719034.4375	705178.4375	730671.125	713992.4375	691448.625	0.007080624
evm.model.chr16.331	687516	703909.375	708559.875	755820.9375	735779.875	734078.0625	-0.083866258
evm.model.chr3.663	814704.0625	677395.3125	643460.6875	786342.625	745445.4375	659256.125	-0.037004106
evm.model.chr3.1139	731978.6875	716119.3125	713819.125	737527.375	700526.25	727873.125	-0.002673233
evm.model.chr3.1140							
evm.model.chr14.278	741358.8125	722469	723818	735571.875	707877.125	723483.5	0.013724966
evm.model.chr4.170	703813.375	702316.75	668519.9375	761823.75	767079.375	763538.8125	-0.144017181
evm.model.chr3.277	732946.4375	703233.9375	794772.5	727303.3125	711511.125	704135.9375	0.058061598
evm.model.chr24.171	686514.4375	725549.125	704026.625	735885.75	760061.625	763317.125	-0.094452066
evm.model.chr2.1475	689114.1875	672950	698865	775846.0625	794374.125	745052.4375	-0.167887146
evm.model.chr2.878.1	761337.5	749984.8125	770528.875	690463.375	705617	709098.9375	0.116261586
evm.model.chr12.159	675801.0625	679349.5	678544.8125	785304.75	793188.625	789310.1875	-0.219445802
evm.model.chr12.554	710676.0625	727262.875	689153.625	748402.25	768204.8125	758639.5	-0.09714008
evm.model.chr20.200	735961.9375	747562.875	735601.625	730129.9375	739949.0625	724163	0.016269222
evm.model.chr22.730	739358.75	732739.3125	731378.875	758041.5625	729965.8125	731546.4375	-0.01048789
evm.model.chr20.696	814144.5625	816951.8125	790180.4375	679144.75	664480.5	673763.5625	0.263278863
evm.model.chr7.19.1	748751.5	783159.25	745231.25	705306.625	737652.875	719829.9375	0.074331043
evm.model.chr11.1130	776725.625	760621.9375	744543.4375	718626.8125	729437.125	734081.1875	0.064482827
evm.model.Contig53_pilon.46.1	695126.75	722033.6875	716718.125	760165.0625	790471.875	783654.9375	-0.129506888
evm.model.chr6.385	744441.8125	725071	731736.875	755630.125	763590.375	749476.375	-0.043541061
evm.model.chr14.499	722370.9375	729826.375	756592.75	759264.0625	775369.9375	749810.0625	-0.048586814
evm.model.chr8.470	764888.3125	763277.125	765538.0625	746849.8125	734134.25	734440.25	0.050095871
evm.model.chr14.146	712998.625	738907.4375	735472.5625	782691.1875	770806.3125	782459.8125	-0.094810945
evm.model.chr10.285	707483.0625	738080.875	711616.5	785489.625	791555.8125	790457.1875	-0.134219169
evm.model.chr11.770	822906.25	710970.8125	725268.3125	793175.1875	753282	723806	-0.007082446
evm.model.chr6.1153.1	773570	747156.25	787122.4375	746552.875	738302.25	737526.75	0.054441899
evm.model.Config706_pilon.3	794250.875	734848.0625	685682.75	786931.375	779631.25	776845.125	-0.081443505
evm.model.chr19.247	713383.625	777105.4375	766108.5	748589	773698.25	782085.625	-0.030225027
evm.model.chr11.978	749517.75	754556.625	718038.9375	793443.4375	773399.125	788040.375	-0.083722958
evm.model.chr13.789	788426.25	766342.0625	793221.6875	755489.0625	754390.4375	739327	0.062010143
evm.model.chr21.502.1	774241.75	739549.625	732139.5	803005.75	781906.6875	766809.25	-0.06640381
evm.model.chr1.846	775169.875	797477.125	765682.125	740676.1875	777908.3125	789829.125	0.018576255
evm.model.chr15.523	100709.0781	1515529.5	104969.625	1635313.875	1310926.125	0	-1.360415836

continue on the next page

**Table S2.** continued

Protein	ML-1	ML-2	ML-3	AL-1	AL-2	AL-3	ML vs ML log <sub>2</sub> FC
evm.model.chr6.423	781358	788982.5625	811454.4375	781126.75	770874.25	749089	0.049731835
evm.model.chr18.70	812799.6875	726709.9375	728506.25	747313.625	850694.9375	818115.8125	-0.091263984
evm.model.chr17.175	791636.0625	787722	786953.4375	788805.125	765148.5625	767566.625	0.027570098
evm.model.chr9.489	775344.75	730475.0625	741751	838557.3125	808916.8125	803405.25	-0.12493291
evm.model.chr22.115	793918	781562.875	763289.9375	783187.375	798747.6875	784174.5	-0.016766387
evm.model.chr6.1370	775175.75	765467.875	778665	802728	796329.125	800861.125	-0.049290454
evm.model.chr9.142	790834.625	796072.625	780499.8125	787798.5	790215.625	786424.625	0.001810021
evm.model.chr1.917	794903.25	763581.375	783890.5	795745.875	807662.8125	787095.3125	-0.029342682
evm.model.chr17.834	764133.25	792688.75	778814.875	799260.3125	792770.5	806328	-0.038231519
evm.model.chr2.525	836061.5625	762781.5625	781722.6875	776049.5	797851.75	780636.625	0.015860584
evm.model.chr22.520	802908.625	784880.3125	795816	807232.1875	791305.25	766955.625	0.011004211
evm.model.Contig746_pilon.2	792242.5	813237.5	814782.8125	785394.75	778838.375	773515.8125	0.050043716
evm.model.chr18.246	800691.3125	796908	801637.375	771459.9375	793919.0625	797846.8125	0.021817999
evm.model.chr3.622	761359.375	746351.875	828324.5625	813403.875	823224.5	809454.3125	-0.066410782
evm.model.chr15.612	782050.875	772382.9375	812192.1875	862155.625	783509.75	773808.3125	-0.031861516
evm.model.chr4.1108	792911.875	825076.8125	818264.8125	780445.125	762971.5625	820294.25	0.043610642
evm.model.chr14.356	849062.75	815461.5	825352.375	770203.4375	781081.3125	788171.25	0.089901163
evm.model.chr17.404	767705.6875	799408.1875	781422.375	820713.1875	839065.0625	837264.625	-0.088458731
evm.model.chr3.365	792880.875	754709.375	772259.1875	872176	838818.875	822114.875	-0.12687841
evm.model.chr5.485	820074.3125	826256.3125	799873.875	798033.875	791736.25	838535.875	0.010594784
evm.model.chr2.1263	807193.5625	799609.6875	774617.25	833352.0625	827684.875	835362	-0.068026115
evm.model.Contig359_pilon.11	784143.4375	821719.9375	879137.375	825289.8125	795810.1875	796681.9375	0.039562155
evm.model.chr16.422	800449.1875	798648.875	791232.0625	833170.5625	843167.625	836481.625	-0.072097343
evm.model.chr9.399	794570	798827.9375	715979.4375	828015.5	873114.3125	924176.3125	-0.184981716
evm.model.chr19.334	772759.0625	817505.3125	850405	859553.4375	878683.625	804243.5625	-0.058959906
evm.model.chr3.11	839157.8125	820818.8125	821198.125	817708.125	851241.625	855532.1875	-0.024964007
evm.model.chr13.467	814616.1875	835422.75	888683	827730.9375	817284.25	839025.75	0.031413438
evm.model.Contig138_pilon.11	807786.125	780275.375	798253.5625	891284.9375	896410.25	865651.0625	-0.15302842
evm.model.chr23.324	800963.25	825727	802263.625	850671.4375	871970.625	890210.625	-0.105290694
evm.model.chr19.224	865498.25	846529.875	846581.9375	840909.25	838859.6875	841657.8125	0.02111998
evm.model.chr7.427	839624.6875	821122	824318.75	907916.9375	855924.25	849727.5625	-0.072737268
evm.model.chr15.715	855058.9375	871335.125	859029.125	838575.8125	843463	839992.4375	0.035814291
evm.model.chr17.598	862911.75	862255.625	853504.3125	857350.3125	842154.625	834545	0.025183148
evm.model.chr13.39	742753.75	839485.25	824102.125	1007655.813	850490	848249.8125	-0.169531575
evm.model.chr8.332	809819.25	844778	847153.75	835899.4375	884531.625	905335.9375	-0.069800698
evm.model.chr15.5	871066.625	835058.875	833376.375	833111.5625	869953.375	906499.625	-0.039263557
evm.model.chr16.660	845862	850759.125	840538.5625	877924.0625	876730.25	881460.875	-0.055199087
evm.model.chr24.39	817667.3125	855118.625	850763	940520.6875	839766.625	873854.125	-0.072791189
evm.model.chr1.502	836362	827610.5	867752.9375	914637	862574.875	869813.625	-0.064251138
evm.model.chr5.529	811805.5	842030.25	849643.9375	893621	903458.4375	886742.375	-0.10035414
evm.model.chr11.705	836573.25	843032.3125	873879.5625	888582.3125	898204.0625	857768.5625	-0.050557291
evm.model.chr2.1558	836351.8125	837019.3125	822356.5625	893966.125	908501.875	900275.4375	-0.11496404
evm.model.chr24.488	1054817	713501.6875	677454.375	1028869.313	1025324.938	702427.25	-0.172610645
evm.model.chr4.202	846060.0625	860413.4375	861821.9375	877101.625	899134.375	869036.875	-0.042605383
evm.model.chr2.565	866584.6875	881366	833840.625	950410.4375	830972.1875	861621.75	-0.033806422
evm.model.chr22.365	714916.6875	873066.375	810769.6875	830210.375	1046852.375	951719.1875	-0.237896508
evm.model.chr13.636	933062.625	898810.4375	903068.8125	858387.3125	856077.25	830420.625	0.103909602
evm.model.chr4.534	920353.3125	888306.8125	913897.1875	838623.5	886165.875	858156.75	0.075944867
evm.model.chr8.776	903775.1875	889098.25	859363.375	887115.8125	890828.3125	881088.1875	-0.003691713
evm.model.chr20.320	882876.4375	895284.375	874703.0625	875226	888507.625	896042.6875	-0.003754271

continue on the next page

**Table S2.** continued

Protein	ML-1	ML-2	ML-3	AL-1	AL-2	AL-3	ML vs ML log <sub>2</sub> FC
evm.model.chr4.1220	901089.25	913938.375	932139.1875	880530.8125	859268.375	838397.75	0.091582047
evm.model.chr14.600	872504.8125	892222	911781.5	853858.25	893255.25	916225.375	0.007116129
evm.model.chr12.158	913147.75	904868.25	872927.8125	859777.625	907135.625	889212	0.018789089
evm.model.Contig352_pilon.2.1	799342.125	907713.5625	872880.25	883922.3125	937741.75	949401.6875	-0.1031057
evm.model.Contig259_pilon.8	855055.25	871416.75	861378.8125	993423.875	888947.9375	896902.625	-0.10295385
evm.model.chr12.29	882445.0625	895701.9375	898070.75	916349.25	875928.0625	909212.3125	-0.013559636
evm.model.chr6.117	914334.3125	927809.6875	891135.3125	873969.875	895466.5	903214.6875	0.032361402
evm.model.chr6.921	885342.5	904410.25	895419.25	917511.3125	924608.5625	916234.5	-0.038793313
evm.model.chr2.1451	913770.125	936017.5625	954891	864458	903164.9375	878424.9375	0.083996336
evm.model.chr16.901	772573.1875	760584	775470.1875	1027260.813	1072790.625	1066567.75	-0.455908049
evm.model.chr1.949	865723.625	854538.6875	860592.875	954244.125	968226.0625	976168.25	-0.167526196
evm.model.chr12.507	904679.1875	917837.6875	912046.9375	932635.25	914929.1875	915473.375	-0.014944577
evm.model.chr19.49	931703.1875	914451.4375	902620.375	945951.875	913125.9375	917287.9375	-0.014408816
evm.model.chr5.359	966346.8125	939703.5625	928809.75	895306.8125	914450.3125	899950	0.065140625
evm.model.chr6.335	905143.25	935790.375	964936.1875	915719.875	925168.625	901080.9375	0.033235581
evm.model.chr6.1149	907308.5	928341.4375	910918.4375	933548.0625	918712.625	950459.375	-0.029197446
evm.model.chr24.26	924385.1875	920794	937597.4375	930545.625	963254.9375	928166.25	-0.020175914
evm.model.chr17.869	921385.375	916430.125	865075	988523.625	935051.375	982118.6875	-0.104379559
evm.model.chr11.583	759439.6875	756625.875	791380.5	1878982.875	698099.25	731953.375	-0.520113845
evm.model.Contig240_pilon.12	1023258.688	1002156	976906.375	882892	868819.375	896127.9375	0.181262691
evm.model.chr10.1227	913207.875	919043.6875	931678.75	953888.8125	956739.8125	979293.4375	-0.064309344
evm.model.chr18.713	908487.9375	917478.5625	885501.25	984459.5	987600.3125	983791.0625	-0.124499475
evm.model.chr4.769	920697.1875	910444.375	944077.4375	932663.875	982208.1875	992956.25	-0.067340468
evm.model.chr16.141.1	978672.6875	975372.8125	909913.75	904121.9375	976905.1875	949740.3125	0.016817736
evm.model.chr18.480.2	1034814.25	1017845.563	1031205.125	862311.625	866821.4375	889187.6875	0.23609774
evm.model.chr11.1039	993337.8125	977823	980862.3125	922332.5625	937231.75	927151.3125	0.083138235
evm.model.chr13.348	981209.4375	972590.3125	960306.3125	977836.8125	974081.5	932688.1875	0.014678858
evm.model.chr18.473	985516.8125	944847.0625	933842.3125	938284	995907.25	1000331.313	-0.034990448
evm.model.chr7.1329	935613.6875	911171.875	912233.625	1000551.125	1032036.5	1011944.625	-0.142065105
evm.model.chr15.719	983568.0625	933702.75	954463.625	1012968.875	966417.5	964972.4375	-0.036031153
evm.model.chr19.254	984696.875	1008120.063	987288.8125	970312.25	946929.25	945867.6875	0.057780836
evm.model.chr6.953	968097.5	962148	964700.125	981813	984182.4375	983850.5625	-0.027103388
evm.model.chr12.1159.1	1204439.625	203519.8125	1190204.25	1095489.875	1086457	1068376.875	-0.3230911
evm.model.chr6.348	950276.8125	957932.75	908409.25	1056255.5	1021057.188	1047824.5	-0.149955193
evm.model.chr11.1229	660957.1875	1146084.625	1212090.125	1010269	809244.25	1160328.375	0.018898149
evm.model.chr7.1478	993448.5625	1030571	1016923.5	964035.0625	1012398.188	1020965.813	0.020807632
evm.model.chr10.366	991505.0625	1000080.688	987736.3125	1029361.563	1012320.25	1027168.063	-0.042713986
evm.model.chr16.555	1153288.125	480395	410173.0625	1312267	1152190.75	1568659.875	-0.980601795
evm.model.chr15.241	1028829.313	1057201.75	1003695	984665.5625	991738.3125	1014735.875	0.046783617
evm.model.chr24.213	1058520.5	1039608.625	1035003.813	1004404.375	978340.1875	974279.6875	0.083459909
evm.model.chr14.160	1386648	988168.0625	971180	1024187.125	997775.75	744889.75	0.274189946
evm.model.chr15.56	1025026.625	1020417.688	1021002.063	1003790.438	1058949.25	1031263.375	-0.012906903
evm.model.chr9.75	994972.6875	992465.75	1008229.438	1063516	1068146.625	1037901.188	-0.081406631
evm.model.chr5.746	1013458.188	997862.25	1004909.125	1058118.125	1052425.125	1042783.063	-0.064128236
evm.model.chr23.443	1029580.125	1064387.625	1057422.375	1003344.5	1011102.063	1012544.438	0.058103978
evm.model.chr2.1452	1104368.875	1081943.25	1086766.25	948970.6875	986172.25	990763.375	0.161764574
evm.model.chr7.1477	1051118.875	1083886.5	1044958.875	998420	1031585.813	1013900.75	0.063086473
evm.model.chr10.956	1072624.625	989936.875	1015804	1051477	1033267.688	1063056.875	-0.032180061
evm.model.chr7.380	1037466.438	1043364.625	1045050.25	1044565.375	1008050.125	1050576.125	0.010510214
evm.model.chr4.169	1019221.563	1049628.5	990188	1037029.688	1048348.063	1090269	-0.053972382

continue on the next page

**Table S2.** continued

Protein	ML-1	ML-2	ML-3	AL-1	AL-2	AL-3	ML vs ML log <sub>2</sub> FC
evm.model.chr14.623	1145346	1033580.688	1025236.688	1001989.375	1020500.75	1038237.5	0.066073046
evm.model.chr24.387	1079812.75	1084889.75	1046434.813	1058571.375	1024606.063	984092.3125	0.066129308
evm.model.chr15.3	1035837.438	1027582.688	1031984.375	1099035.875	1093743.125	1032634.438	-0.059356149
evm.model.chr23.57	1007482.25	1086690.375	1071432.875	1058051.125	1059574.875	1041916.313	0.002765891
evm.model.chr11.1253	1054225.625	1048978.5	1024833.313	1086363	1049187.875	1064579.5	-0.032872903
evm.model.chr19.152	1067076.625	1097837.875	1115436.625	1012905.375	1034505.188	1027664.5	0.09322862
evm.model.chr10.565	1046268.688	972172.5625	955530.8125	1190307.25	1136674.125	1079806.75	-0.196021131
evm.model.chr15.889.2	1156882.125	1134181	1107762.5	1012657.375	1009172.75	1003230.25	0.168072411
evm.model.chr13.608	1137653.25	1139691.75	1134034.75	994381.6875	1010967.438	1010042.625	0.178009918
evm.model.chr17.936	954890.75	1038500	1044958.875	1163923.375	1154116.5	1105373.75	-0.172147721
evm.model.chr2.700	1071285.875	1040105.125	1155854.875	1143218.75	1013149.938	1064434.25	0.020654635
evm.model.chr2.1596	982738.1875	1057384.75	1041663.625	1120623.25	1145159.625	1149887	-0.148401597
evm.model.chr8.366	1120844.625	1153087.375	1038613.625	1025417.188	1105757.875	1069871.625	0.049396607
evm.model.chr6.493.1	1174192	1177344.25	1135021.625	1029422.688	1022221.063	1017837.5	0.183808573
evm.model.chr2.930	1100931	1105175.375	1126660	1060033.25	1089836.75	1081702.875	0.044483663
evm.model.chr23.301	1119384.375	1106227.625	1055406.125	1128499.75	1086640.25	1083344.75	-0.007659871
evm.model.chr9.352	982383.125	972398	1011148.25	1223664.875	1184925.25	1210177	-0.287014026
evm.model.chr12.219	1096474	1057351.25	1061992.25	1098288.375	1145323.5	1136207.25	-0.071760506
evm.model.chr6.1223	1153427.875	1163865.5	1180619.5	1044778.313	1030894.438	1031740.5	0.17078024
evm.model.chr20.535	1110144.5	1121278.625	1092393.125	1179893.375	1114770.875	1081906.25	-0.022718052
evm.model.chr20.694	1206887.125	1096569.5	1158269.375	1118194.75	1067747.625	1057072.625	0.094155841
evm.model.chr14.263	1148306.75	1132631.375	1090776.5	1006095.438	1141051.5	1192621.75	0.01373425
evm.model.chr17.140	1063259	1095232.75	1090488.375	1143770.875	1179773.375	1154693.25	-0.098369527
evm.model.chr14.304	1125999.125	1079836.75	1059503.75	1150796.5	1162628.375	1161630.75	-0.089803018
evm.model.chr4.996	1099807.125	1109894.5	1082840.125	1107871	1187673.375	1165327.125	-0.071933642
evm.model.chr13.892	1173776.375	1092186.625	1111389.75	1157062.125	1087527.625	1136898.5	-0.00176547
evm.model.chr16.423	1332681.125	1172134.5	1228783.125	653978.5625	1286822.5	1105047	0.293722912
evm.model.chr9.59	985143.9375	974539.9375	981340.5625	1322571.125	1308443.875	1285701.75	-0.413326027
evm.model.chr15.868	1175305.125	1149609	1134860.875	1196811.5	1084746	1158829.375	0.008107411
evm.model.chr6.520	1112321.25	1117713.625	1109882.375	1212294.875	1194734.25	1164507.875	-0.096732708
evm.model.chr19.238	1153152.25	1114479.625	1099325.625	1208218.125	1224068.75	1157393.25	-0.092409781
evm.model.chr10.1075	1010495.063	1029952.063	1010633.875	1288089	1326216.25	1326341.125	-0.36911181
evm.model.chr15.127	1157188.125	1140013	1139674.875	1151295.625	1185433.25	1234109.375	-0.055164984
evm.model.chr14.384	1103395.5	1217340.375	1181027.625	1113653.125	1174064.125	1226045.75	-0.004935235
evm.model.chr4.1151	1117241.375	1144891.75	1130229.625	1229356.25	1219837.75	1224168.25	-0.114810727
evm.model.chr19.234	1171663.375	1157341.5	1184983.875	1186617.625	1182856.25	1182549.75	-0.015531605
evm.model.chr6.179	1157502	1178429.25	1181714.375	1188690.75	1143718.375	1219885.5	-0.014141093
evm.model.chr5.466	1247134.75	1227715	1229847	1166358.375	1140134.25	1095648.625	0.122912415
evm.model.chr6.749	1182949.875	1168520.625	1168731.25	1195684.875	1221434	1190562.625	-0.035413862
evm.model.chr18.66.1	1139149.5	1160164.625	1131471.875	1293281.5	1231730.5	1216386.75	-0.125038595
evm.model.chr3.1467	1712515.25	34349.60938	39607.50781	1829802.5	1859388.875	1775214	-1.612950915
evm.model.chr18.286	1195072.375	1188548.125	1114569.75	1248903.75	1277295.5	1275471.25	-0.120024743
evm.model.chr2.1047	697864.5625	1164517.375	1323557.75	1593965.25	1184096.375	1346648.25	-0.372573691
evm.model.chr6.1408	1163790	1179171.625	1200591.375	1258228.75	1228352.75	1289494.5	-0.091691174
evm.model.chr14.212	1266164.875	1220469.5	1222717.375	1217936.875	1169439.75	1247539	0.029245206
evm.model.chr17.121	1119386	1130499.625	1125534.375	1339661.25	1357496	1277494.75	-0.235761525
evm.model.chr2.535	1205895.75	1205385.125	1205318	1250969.875	1249986.625	1243484.375	-0.050116715
evm.model.chr2.533							
evm.model.chr23.506	1184005.125	1200570.75	1156561.75	1293125.375	1313199.125	1226414	-0.114162655
evm.model.chr17.830	1307718	1302451	1296260.625	1157962.75	1177046.625	1150000.75	0.164687776
evm.model.chr2.572	1212805.625	1177173	1208534.75	1222486.75	1314225	1263714.5	-0.078760218
evm.model.chr10.319	1205388.375	1168519.5	1164073	1316247	1283096.75	1282478	-0.133807623

continue on the next page

**Table S2.** continued

Protein	ML-1	ML-2	ML-3	AL-1	AL-2	AL-3	ML vs ML log <sub>2</sub> FC
evm.model.chr3.480_evm.	1245270	1208689	1172032.375	1262603.125	1271519.375	1263507.5	-0.066723858
model.chr3.481_evm.							
model.chr3.482							
evm.model.chr23.271_evm.	1289952.5	1201447.875	1163482	1312139.5	1262224.375	1241257.25	-0.062092948
model.chr23.272							
evm.model.chr18.734	1484087.875	1277845.5	1282774.125	1140487.75	1170748.125	1151743	0.224021789
evm.model.chr3.413	1252606.25	1207551.25	1247532.625	1278396.125	1252553.75	1276320.5	-0.038236353
evm.model.chr3.184	1210929	1203170.875	1234119.875	1296391.5	1302621.125	1300161.625	-0.095975996
evm.model.chr7.1228	1405589.125	1435501.125	1440599.875	1080645	1083840.5	1105698.875	0.388808411
evm.model.chr6.893	1206129.75	1233114.25	1221162.5	1256776.125	1342418.5	1322629.75	-0.099521058
evm.model.chr4.1374	1220570.375	1280870	1293331.75	1236149.5	1274592.5	1301435	-0.006601851
evm.model.chr5.436	1276507.625	1304868.25	1270089.5	1254686.75	1258038.375	1247726.875	0.034501374
evm.model.chr22.656	1180099.625	1343903.375	1403802	1037154.313	1408434.375	1265783.125	0.081770767
evm.model.chr10.67.1	1311515.125	1285295.125	1288666	1248626.375	1264404.875	1257966.75	0.043145058
evm.model.chr21.414	1211342.625	1248803.75	1218457.125	1335160.625	1371811.5	1390776	-0.155673126
evm.model.chr15.34	1270434.25	1226084.125	1230125.875	1342651.125	1355615.375	1361230.875	-0.123424008
evm.model.chr7.624	1136778.75	1146546.625	1252909.125	1431308.5	1400558.875	1443781.375	-0.273929391
evm.model.chr19.325	1241728.875	1236970.25	1243205.75	1393357.5	1341121	1363065.75	-0.138718346
evm.model.chr18.617	1255840.875	1334547.125	1354523.25	1318753.25	1299309.25	1276671.875	0.018467905
evm.model.chr7.740	1334543.75	1289929.875	1309217.625	1309435.75	1302885.375	1306573.875	0.005436808
evm.model.chr10.1247.1	1128334.625	1178260.25	1138363.375	1475877.5	1459936.875	1475615.375	-0.356759812
evm.model.Contig72_pilon.22	1295326.625	1335347.625	840874.125	1412080.25	1568023.375	1418813.5	-0.341569146
evm.model.chr15.440	1251394	1228341.5	1273010	1380430	1377897.5	1381062.75	-0.141471814
evm.model.chr3.379	848232	1423538.25	1336246.5	1411979.25	1393379.75	1504969.125	-0.256591663
evm.model.chr18.247	1292409.75	1288124.125	1328148	1351488.875	1334210.625	1333089	-0.040078484
evm.model.chr18.98	1338406.125	1255800	1271918.875	1378340.75	1392591.625	1360155.875	-0.095633596
evm.model.chr1.1068	1369588.625	1333674	1345760.25	1342334.625	1339131.75	1269951	0.035203552
evm.model.chr4.1165	1334618.5	1330878.625	1301194.25	1345124.375	1357150.25	1349391.5	-0.03057914
evm.model.chr10.1115	1361064.625	1334330.125	1352608.625	1349069.875	1349222.625	1351426.375	-0.000611269
evm.model.chr3.934	1435910.625	1369129.25	1349846.625	1301627.5	1320312.625	1326145.375	0.073655834
evm.model.chr10.278	1327353.25	1367853.25	1359865.25	1360782.875	1350016.625	1354949.625	-0.003793756
evm.model.chr18.829	1420340.5	1447809	1404717	1322234.25	1261124.25	1277483	0.146288914
evm.model.chr9.1145.8	1214520	1320749	1504065.125	1511077.875	1284290.125	1328091	-0.029737575
evm.model.chr17.30	1450975.875	1395777.625	1327211.375	1364891.75	1317924.5	1353195.375	0.04848813
evm.model.chr22.486	1353444.625	1324793.125	1316513.375	1475084	1362052.125	1378136.375	-0.077520273
evm.model.chr13.356	1375986.25	1373079.5	1347869	1387387.875	1377126.75	1352672.5	-0.007114104
evm.model.chr7.111	1334934.25	1371854.5	1314929	1378852.75	1385991.875	1435027.125	-0.062533439
evm.model.chr19.630	1302381.375	1371587.75	1377473.25	1410325.75	1395934.125	1398753.125	-0.05367464
evm.model.chr1.1028	1363081.625	1382087.375	1356871.875	1386551.5	1383962.5	1392001.75	-0.021113863
evm.model.chr8.308.3	1366464.875	1365806.375	1353569.625	1365062.5	1418884.375	1411423.625	-0.038165204
evm.model.chr2.798	1398121.125	1319082.25	1321406.375	1473083.625	1420095.375	1428831.875	-0.097843957
evm.model.chr15.891	1389166.375	1401250.5	1416648	1386006	1430373.625	1395147.875	-0.001529521
evm.model.chr1.1005	1463308.625	1460590.25	1475277	1359198.875	1353219	1324458.5	0.123993874
evm.model.chr8.178	1451915.75	1349344.125	1389046.125	1402157.125	1409317.5	1444755.125	-0.022520428
evm.model.chr3.1428	1334937.375	1359803.625	1342037.75	1470040.25	1494063.125	1510831.5	-0.14866217
evm.model.chr23.246	1486559.125	1441601.75	1421695	1449877.125	1411640.25	1372115.75	0.039071346
evm.model.chr12.1122	1519025.25	1531851.5	1468334.25	1372715	1313909.25	1386003	0.150111141
evm.model.chr12.513.1	1481872.375	1434308.25	1079098.5	1532524.25	1545050	1553781	-0.213138125
evm.model.chr21.173	1407970.75	1423672.125	1363779.25	1523006.25	1489060.75	1462020.875	-0.092777617
evm.model.chr1.1045	1495199	1504594.25	1534018.5	1380784.25	1388425.625	1368039.625	0.132052527
evm.model.chr19.708	1490292.375	1503998	1510454	1444879	1378941.125	1415266.75	0.087691709
evm.model.chr7.1244	1455254.25	1387535.625	1384559.625	1516696.625	1512336.875	1506273.375	-0.101446778
evm.model.chr18.869	1546629.5	1522311.125	1513759.25	1458283.75	1372376.125	1374616.625	0.123997144

continue on the next page

**Table S2.** continued

Protein	ML-1	ML-2	ML-3	AL-1	AL-2	AL-3	ML vs ML log <sub>2</sub> FC
evm.model.chr6.806	1482408.5	1438638.125	1464344.5	1514313.5	1495766.25	1468454.125	-0.030320999
evm.model.chr17.619	1632577.375	1387997.75	1317550.125	1671217.5	1225473.125	1642466.875	-0.065352841
evm.model.chr9.370	1519805.75	1499545.125	1472053.625	1512926.625	1478631.75	1427446.125	0.023445258
evm.model.chr1.864	1520615.125	1495977.5	1512104.375	1444412.25	1448796	1490353.625	0.046992405
evm.model.Contig228_pilon.7	1511331.125	1567726.125	1580011.875	1420384	1430107.75	1435300.375	0.120479859
evm.model.chr17.667	1576893.5	1604573.625	1577643.875	1395233.75	1462319.75	1390561.875	0.163869155
evm.model.chr17.662	1470976	1487431.875	1465926.875	1561212.25	1514279.25	1533135.125	-0.058876345
evm.model.chr1.1009	1570584.625	1539617.5	1484104.125	1482104.75	1495311.875	1466084.875	0.048150053
evm.model.chr17.729.3	1454004.375	1510296.5	1504499.75	1527630.5	1544330	1561794.5	-0.052294086
evm.model.chr11.587	1453733.5	1417509.25	1412409.625	1590508.625	1649885.125	1592691.75	-0.174103109
evm.model.chr19.308	1470943.75	1484975.875	1436236.875	1602949.5	1587291.25	1545249.625	-0.108584368
evm.model.chr21.394	1460433.5	1431883	1446509.125	1629680	1601216	1582719.625	-0.149816339
evm.model.chr11.1363	1521627.25	1509818.75	1475757.125	1573614.125	1544626	1538658.75	-0.047137085
evm.model.chr9.1025	1443627.625	1435240.75	1436042.5	1534259.75	1612716	1703590.125	-0.168822304
evm.model.chr23.444	1541093.5	1532274.5	1521034	1596347.375	1561319.125	1515417.625	-0.024497914
evm.model.chr1.359	1480034.75	1456704.125	1430684.875	1638045.25	1650497.875	1621505	-0.168954649
evm.model.chr5.349	1520205.875	1561342.125	1642250.75	1500549.5	1571922.125	1525728.875	0.038878128
evm.model.chr19.263	1524956.5	1526402.875	1576386.875	1617425	1560360.125	1599850.25	-0.045986992
evm.model.chr24.453	1489659.75	1552949.5	1549226.625	1526916	1638235.125	1651680.375	-0.06901338
evm.model.chr7.623	1356133.375	1348137.625	1295121.125	1781975.375	1895368.375	1811370.25	-0.456687428
evm.model.chr23.185	1515365.5	1527524.375	1482765.5	1645192.75	1701046.625	1647529.125	-0.142002214
evm.model.chr5.149	1586497.75	1638919.75	1639007.25	1722058.875	1782798	1771463.25	-0.117262891
evm.model.chr14.549	1725132	1663009.875	1695184	1660881	1712836.625	1684725.125	0.007079403
evm.model.chr22.361	1649259.75	1645985.5	1649258.625	1792392	1752941.375	1731706.875	-0.093903217
evm.model.chr3.165	3451054.75	3375108.75	3312039	123586.2188	5578.225098	13865.31934	6.147342686
evm.model.chr6.380	1729418.875	1743250.875	1686127.625	1741387	1732768.625	1678614.25	0.00168662
evm.model.chr1.430	1755334.875	1799663.125	1737570.5	1546196.125	1776696.625	1779609.875	0.052763017
evm.model.Contig130_pilon.7	1772544.875	1834593.75	1793602.5	1602369.375	1723172.375	1707965.5	0.101593405
evm.model.chr11.542	1702681.875	1686893.125	1684083.75	1787493.125	1842827.75	1782217	-0.093278727
evm.model.chr6.160	1742572.625	1628319.125	1614558.75	1865063.375	1806654.875	1876011.5	-0.154173634
evm.model.chr14.400	1762853.375	1755077.5	1767787.5	1746135.625	1772481	1758026.125	0.002479249
evm.model.chr23.520	1710591.875	1667037.25	1667447.625	1858748	1851031.25	1856804.25	-0.141915926
evm.model.Contig340_pilon.23	1718320	1783142.875	1778935.375	1858271.125	1826264.5	1784711.25	-0.050695443
evm.model.Contig575_pilon.21	1801634.625	1785738	1823789.625	1809797.25	1803597.75	1754290.125	0.011638456
evm.model.chr14.502	1667042.75	1773089.875	1915636.625	1765155.125	1848908.625	1828065.875	-0.023077516
evm.model.chr6.976	1856846.5	1829226.375	1744428	1708368	1803748.375	1858472.25	0.016005051
evm.model.chr7.1045.1	1793228.625	1815900.25	1788438	1818119.875	1792055.625	1802353.875	-0.003993737
evm.model.chr11.738	1985704.5	1818135.25	1761653.875	1815262.25	1838294.5	1897891.25	0.003645529
evm.model.chr4.561	1704664.375	1727845.625	1696401.5	2015983.375	2033829.75	1986393.875	-0.234989603
evm.model.chr2.1008	1826842	1835199.5	1795522.375	1923702.5	1909890.25	1894932.125	-0.069906575
evm.model.chr9.272	1799481.375	1835859.5	1800539	1927444.625	1887418.75	1952474.25	-0.085391906
evm.model.chr20.430	1899172.5	1870492.75	1809114	1903332	1908151.625	1868963.25	-0.026054964
evm.model.chr12.747	1883046.75	1852645.625	1834425.25	1916628.625	1924272.375	1869228.875	-0.035815766
evm.model.chr10.664	1870929.625	1849879.75	1843888.25	1931451.5	1905134	1894029.875	-0.042386773
evm.model.chr5.269.1	1733496.125	1715718.5	1673091.375	2032728.75	2052254.75	2093724.875	-0.270511842
evm.model.chr10.779	1743708.625	1762870.5	1753068.5	2091367.25	1999556.5	2015030	-0.215250514
evm.model.chr19.282	1839326.75	1911999	1915075.5	1912567.5	1954363.875	1941877.875	-0.03580969
evm.model.chr19.429	1836804.5	1558956.25	1302833.75	2479724	2080957.125	2351237.75	-0.55685702
evm.model.chr2.979	1941226.625	1955114.25	1769553.875	1884199.5	2123659.75	1940756.75	-0.070250249

continue on the next page

**Table S2.** continued

Protein	ML-1	ML-2	ML-3	AL-1	AL-2	AL-3	ML vs ML log <sub>2</sub> FC
evm.model.chr17.734	1882881.25	1980304.375	1955321.5	1955775.875	1994912.75	1895392.625	-0.006820837
evm.model.Contig127_pilon.15	1944026	1929473.25	1927550.875	1952282.25	1961061.875	1952383.375	-0.015995965
evm.model.chr12.950	1900772.25	1888014.75	1910241.5	2015163.375	2041994.375	2012439	-0.090884663
evm.model.chr8.961	1921681.875	1942131.625	1918122.625	2085827.625	2016532.625	1978989.75	-0.072838952
evm.model.chr22.140	1869976.375	1929136.875	1945065.75	2087659.875	2054051.375	1980084.75	-0.091854263
evm.model.chr11.534	1913085	1948323.25	1946253.875	2028930.875	2031084.875	2000622.375	-0.06151218
evm.model.chr1.946	1860684.5	1921775.25	1911773.625	2044036.625	2081871.75	2071684.125	-0.122206277
evm.model.chr1.633	2028100.25	2094683	2099176.5	1922763.125	1875095	1886484.625	0.130375514
evm.model.Contig219_pilon.8	2108405.5	2107008	2175189.25	1884799	1843990.125	1838388.625	0.199005863
evm.model.chr11.1119	1963951.25	2035478	2003135.875	2040867.75	1983691.75	1978911.125	-0.000217617
evm.model.chr12.34.1	2991871.5	2077633.625	2068394.875	2979883.5	22573.84961	1909559.625	0.539184143
evm.model.chr6.601	2078528.5	2054724.25	2036012.375	2001448.375	1982500	1951990	0.055622533
evm.model.chr2.742	1872029.25	1864886.125	1869352	2164908.75	2161231	2176984.25	-0.214092382
evm.model.chr9.60	2000829.375	1962996.5	1954540	2115325.5	2076287.5	2069623.25	-0.081248651
evm.model.chr12.162	1982857.375	2124632	2134197.5	2009737.375	1940147.625	1994931.125	0.070303796
evm.model.chr17.825	1989442.25	1970766.75	1908963.625	2126422.75	2173004.25	2103035.75	-0.125469813
evm.model.chr9.885	2110334	2059330	2031132.375	1950482.875	2089869.75	2030959	0.030445289
evm.model.chr7.518	2134855	2036498.75	2018987.5	2057033	2031572.875	2007902.25	0.02203579
evm.model.chr1.1199	1922089.125	1949788	1941916.875	2166621.75	2181766.25	2136839	-0.15767712
evm.model.chr23.521	1951423.25	1889291.5	2033149.875	2195574.25	2177841.75	2073263.25	-0.134246189
evm.model.chr16.191	2098526.25	2080583.75	2078690	2055458.25	2093870.5	1975125.75	0.0310742
evm.model.chr15.890	2038642.25	2022282.875	2025566.625	2041501.625	2135265	2218827	-0.071467374
evm.model.chr9.1236	1975906.5	1929619.5	1970395.375	2236911	2201836	2206910.75	-0.177596905
evm.model.chr15.722	2119258.5	2113522	2029487.25	2098308	2113615.5	2061923.125	-0.002665067
evm.model.chr3.769	2141077.5	2080402.75	1951955.125	2134085.5	2140261.75	2134442.25	-0.053978345
evm.model.chr1.1071	2189596.75	2088805.75	2041045.625	2107698.5	2087041.375	2079437.125	0.010372344
evm.model.chr4.1110	2140565.5	2130100	2143976.25	2122940.25	2111080.25	2124608.75	0.012652902
evm.model.chr15.881	2199845	2180863.5	2199251.25	2103472.75	2134348.5	2146432	0.043560878
evm.model.chr6.1142	2200049.75	2196061.75	2147556.5	2204245.25	2143360.5	2073758.75	0.02721966
evm.model.chr5.724	2885479.5	2817491.5	0	2571009.75	2384336	2376516.25	0.222496565
evm.model.chr1.1193	2061793.75	2316819	2382646.75	2021077.75	2136551.75	2152747.75	0.099565764
evm.model.chr1.1194							
evm.model.chr2.1634	2209941.25	2186439.5	2205945.75	2184459.75	2165883	2224239	0.006075366
evm.model.chr17.334	2018970.375	2537476	2117294	2204333.5	2195264.5	2181349.5	0.020200251
evm.model.Contig800_pilon.9	2338924.5	2405606	2395866.25	2100690.75	2124961	2050170.875	0.186199661
evm.model.chr11.40	2260399	2201473	2228529.25	2303732.5	2215687	2210459.5	-0.008487828
evm.model.chr7.264	2299357	2257440	2198553.75	2324406	2334953.5	2317734.5	-0.046595592
evm.model.chr8.657	2311185	2380093	2479458.25	2203363.5	2176437.5	2286739.25	0.105183017
evm.model.chr4.557	2280303	2289568.5	2302106	2451823	2415254.5	2394519	-0.079561454
evm.model.chr17.895	2323029.75	2269384.25	2235900	2435226.75	2464973.75	2483253.5	-0.112766469
evm.model.chr2.976	2247380.75	2347238	2351449.75	2429287.25	2501982.5	2420983.75	-0.081989872
evm.model.chr4.838	2267689.75	2343772.25	2314302	2458196	2501796.25	2505249.5	-0.108215753
evm.model.chr18.435.2	2460024	2505940.75	2530644	2364165.5	2374366.25	2332251.5	0.084368074
evm.model.Contig294_pilon.5.1	1610937	2546018.5	2524727	2697601	2653159	2637169.75	-0.257610215
evm.model.chr6.1242	2433183.25	2441655	2434964.5	2431228.25	2452658.25	2488353.25	-0.012270513
evm.model.chr10.828	2486809.5	2505025.5	2536476.25	2313233.5	2435248.75	2426751.75	0.069300394
evm.model.chr1.618	2445796	2475834	2511252	2386683.5	2396589	2507154.5	0.027918389
evm.model.chr22.324	2305171	2332180.25	2333964.75	2625286.75	2538225	2612687.75	-0.157634208
evm.model.chr2.1442	2436300.75	2439643	2488997.75	2470441.5	2488840	2429431	-0.004648927
evm.model.chr3.237.3	2438923.75	2463187	2522213.75	2498027.75	2515000.5	2478334.25	-0.012968366

continue on the next page

**Table S2.** continued

Protein	ML-1	ML-2	ML-3	AL-1	AL-2	AL-3	ML vs ML log <sub>2</sub> FC
evm.model.chr19.147	2460763	2454716.25	2546517	2551987.75	2503727.5	2436445	-0.005820123
evm.model.chr10.940	2337994	2358182	2447138.75	2637937.25	2603940.5	2586093.75	-0.132044812
evm.model.chr11.641	2529685	2517791.5	2464146.75	2546316.75	2552844	2504528.25	-0.01757482
evm.model.chr6.850	2319875	2343704.5	2413021.5	2688496.25	2737379.5	2643153.5	-0.189338541
evm.model.Contig359_pilon.10	2562925.5	2567615.25	2469094.75	2639960	2509225.75	2434620.75	0.00300807
evm.model.chr4.1144	2515598.5	2459420.75	2448593.75	2604651.25	2571325	2615776.25	-0.069826349
evm.model.chr22.690	2546980.75	2506496.25	2398623.5	2599264.25	2619404	2570550	-0.063831411
evm.model.chr1.767	2514302.75	2488591.25	2557203.25	2629954	2554944.75	2504885.5	-0.024538329
evm.model.chr2.1546	2596771.25	2610830.25	2503953	2500178.75	2590599.75	2614501.25	0.001174372
evm.model.chr20.143	2555797.75	2533437	2530911.75	2539624.5	2662577.25	2607303	-0.035412327
evm.model.chr2.1202	2619637.75	2521721.5	2565199	2614955	2577100	2618581.75	-0.01935347
evm.model.chr6.269	2558644	2525483.5	2557083.5	2641501.5	2646746.75	2622695.25	-0.05004847
evm.model.chr17.866	2602099	2611902.75	2531844.5	2720064.25	2600072.75	2718195.25	-0.053473345
evm.model.chr18.666	2491873	2520228.75	2534754.75	2778888.75	2725381	2767262	-0.132278675
evm.model.chr21.285	2675682	2698751.25	2724889.75	2601745.75	2589126	2593702.25	0.05718323
evm.model.chr3.423	2660940	2704638.25	2586743.5	2731886.75	2623791.25	2615191.5	-0.003360979
evm.model.chr3.89	2448392	2418292.5	2456531.5	3030637.5	2819774.25	2795618.25	-0.239560493
evm.model.chr6.811	2683353.25	2763957.5	2641649.25	2619601.5	2663860	2613935	0.034577102
evm.model.chr20.442	2683246	2520446.5	2631384	2721621.5	2763010.5	2710564.5	-0.064831181
evm.model.chr4.262	2691468.75	2555369	2619799	2778970.5	2788508.25	2708363.75	-0.073159222
evm.model.chr6.652	2548066.5	2666423	2594300.5	2748769.5	2826293.75	2770525	-0.095914729
evm.model.chr8.1074	2632698.25	2539154	2546691.5	2872559.5	2749192.5	2852985.5	-0.134840001
evm.model.chr13.750.1	2578666.25	2529421.5	2542994.75	2873123.75	2845642	2856310	-0.164485536
evm.model.chr7.1229	2639042.5	2671971	2683178.5	2733233.5	2773400.5	2760086.75	-0.04836293
evm.model.chr3.235	2572992.5	2561990.25	2452929.25	2927995.75	2924931.75	2855730.75	-0.198747511
evm.model.chr20.443	2659142.5	2637105.5	2614336.25	2867452	2827006	2873824.5	-0.115221796
evm.model.chr12.472	2657180.5	2592859.75	2720072	2925257	2822744	2898149	-0.117457822
evm.model.chr4.1164.1	2837456.5	2813194	2865376	2745305.25	2670275.75	2821598.75	0.048029968
evm.model.chr2.944	2881888.75	2964584.25	2879672.25	2764872.75	2764138.75	2708076.5	0.083210086
evm.model.chr16.740	2780313.75	2791390.5	2785547.75	2903083	2826003	2952081.5	-0.05486044
evm.model.chr13.267	2745295.75	2756504.25	2812722.5	2945169.5	2864174	2935242.25	-0.07275663
evm.model.chr1.601	2719325.25	2773595.75	2733894.25	3012525.75	2992626.25	2868433.25	-0.109183078
evm.model.chr1.509_pilon.1	2975493	2908993.5	2862985.75	2711684.5	2857549	2883807.25	0.049395778
evm.model.Contig141_pilon.1	2960414.75	2926016	2906063.75	2794003	2804026	2819180.75	0.062930459
evm.model.chr13.2	2558448.75	2679958	2593864.5	3181302.25	3104106.5	3172951.75	-0.272159401
evm.model.chr7.1116	2989459	3084798.25	2963237.5	2755786.5	2740225.5	2785920.5	0.12595546
evm.model.chr7.1075	2796985.25	2672731.25	2674198.5	3143668.25	3067940.25	3091502.5	-0.191990737
evm.model.chr3.683_pilon.6	2874572.5	2841967.5	2824083	2994655.75	2951447.25	2966807.5	-0.061555307
evm.model.chr14.168	2730939	2795355.5	2756941.75	3035993.25	3094713.5	3058786.5	-0.14979077
evm.model.chr5.315	2882996.25	3001238	2910383.5	2926998.5	2994080	2893434.5	-0.00325999
evm.model.Contig259_pilon.6	3049776.5	2887404	2900845.5	2952390.75	2948832.5	3030405.25	-0.01519907
evm.model.chr14.766	2822198.25	2844375.25	2807741.5	3092458	3135965.5	3155205	-0.147049142
evm.model.chr5.160	3011499.5	2986057.75	2992493.25	2996240	3044538.5	2968141.75	-0.003024985
evm.model.chr6.53	2868559.5	2839992	2778840.25	3240764.25	3183131.25	3130694.25	-0.17087266
evm.model.chr16.376	2705866.75	2912022.5	2803232.75	3308802.5	3258518	3162918.25	-0.208462739
evm.model.Contig205_pilon.19	3055154.25	2967671	2864797	3201768.75	3044361.5	3036923	-0.062801895
evm.model.chr12.168	3519719.25	2783463.5	2775140.25	3140837.75	3012996	2988682.5	-0.010165467
evm.model.chr11.1106	3153772	3114887	3099413	2982059.5	3094381	3070728.5	0.034426858

continue on the next page

**Table S2.** continued

Protein	ML-1	ML-2	ML-3	AL-1	AL-2	AL-3	ML vs ML log <sub>2</sub> FC
evm.model.chr17.946	3039059	3063243.5	3042458.5	3148340.5	3187695	3172299.75	-0.056247306
evm.model.Contig455_pilon.11	2833461.5	3151242	3019125.5	3274822	3242648.75	3132309.25	-0.099957394
evm.model.chr16.13	3023863.5	3114027.5	3134625.75	3104687.5	3216686	3074916.75	-0.01913031
evm.model.chr21.470	3071243.5	3125909.25	3128631.5	3233991.75	3215813.5	3174106.25	-0.045398322
evm.model.chr12.1221	3120963.75	3051979	3110723.75	3313191	3342900.25	3312457.25	-0.102688755
evm.model.chr22.487	3283989.75	3191283.5	3269401.75	3144984.25	3264549.75	3207929.5	0.018957621
evm.model.chr9.470	3282615	3113198.25	3221278.75	3284632.5	3345795.75	3187751.5	-0.029854859
evm.model.chr6.933	2968840.25	3051809	3041390.75	3448960.75	3509490.75	3455384.25	-0.200593793
evm.model.chr14.151	3061812	3064742.25	3000957.75	3475440.5	3468155.5	3424682.5	-0.18388281
evm.model.chr2.981	3226458.5	3152325.25	3127177.5	3359794.5	3427468.75	3473899.5	-0.110289794
evm.model.chr18.405	3588841.25	3116776.5	3186967.75	3388118.75	3290360.5	3214026.75	1.1594E-05
evm.model.chr13.227	3151257.25	3201471	3176391	3484095	3449612.5	3363081	-0.111779659
evm.model.chr12.325	3373763.25	3205950	3123687	3410762.75	3419322.25	3430952.5	-0.080614322
evm.model.chr11.506	3283177.25	3207018.25	3187534.25	3413300.75	3437313.25	3535372	-0.101897628
evm.model.chr7.888	3575311.5	3576712	3419584.5	3110227.25	3167388	3221938	0.154263263
evm.model.chr6.167	3395018.25	3373100.25	3429137.75	3367823.25	3295503.75	3260875.5	0.039157944
evm.model.chr15.741	3167867	3160260.5	3044798.25	3726421.75	3613800.25	3570567	-0.219184073
evm.model.chr1.1233	3256442	3170838.75	3171305.75	3635966.25	3610843.75	3547824.5	-0.169420522
evm.model.chr3.83	3338310	3287918.5	3269667	3509586.5	3579842.25	3449803	-0.090867536
evm.model.Contig80_pilon.37	3246119.75	3362660.5	3251774	3507384.25	3588139.75	3582421	-0.114893377
evm.model.chr18.570	3584315.75	3392514.5	3401126.5	3490003	3545365.25	3493862	-0.020877542
evm.model.chr19.428	3504128.75	3556846.5	3679862	3311061	3504822.5	3455670.5	0.06445199
evm.model.chr15.206	3381109.75	3377975.25	3442685.75	3597078.5	3666674.5	3592425.25	-0.089696727
evm.model.chr20.786	3582393.75	3617724.75	3469252.75	3474191	3498362.75	3496326	0.027368089
evm.model.chr12.718	3477191.5	3433525.5	3476319	3508638.25	3682751.5	3624498.5	-0.058368119
evm.model.chr17.534	3429923.25	3550837.75	3411601.25	3643580	3603485.5	3565934.5	-0.05724322
evm.model.chr24.243.2	3526000.5	3473434.75	3586504.75	3696905.75	3543969	3618795	-0.036830848
evm.model.chr24.532.1	3383071.25	3452251.75	3518258.25	3802790.75	3719795	3579887	-0.100751156
evm.model.chr2.179	3441849	3507931.75	3538078.75	3819386.75	3535402.5	3767636.75	-0.084751236
evm.model.chr1.1007	3483445.25	3600114.25	3651489	3600397.25	3740762.5	3608738.25	-0.028588722
evm.model.Contig124_pilon.24	3651487.5	3563842.25	3533187.25	3580719.25	3705311	3797302.75	-0.044254175
evm.model.chr15.505	3540063.75	3671777.75	3529007	3756540.25	3621948.75	3722205.75	-0.047542005
evm.model.chr7.1384	3595630	3662815	3663774.5	3797319	3666024.5	3752533.5	-0.038276378
evm.model.chr15.698	3864620.75	3837538	3839346.25	3629740.75	3688907.5	3620040.75	0.07739152
evm.model.chr4.7	3789750	3793382.5	3779751.25	3826366.5	3757092.5	3806488.5	-0.003432079
evm.model.chr9.1240	3789974	4037284	3703573	4015619	3868103.75	3701606.75	-0.006802588
evm.model.chr3.295	3746167.75	3890686	3827908.5	3940705.75	4037250.5	3947160	-0.056796893
evm.model.chr9.302	4054716.75	4026317.25	3921769.75	3819530.25	3843607.75	3861159.75	0.058692606
evm.model.chr13.56	3917322.5	3859731.75	3906696	4044768.5	3870182.25	3942730	-0.021318435
evm.model.chr22.337	3874548	4021434	4014922	3962414.5	4033979.25	4054640.5	-0.016874054
evm.model.chr3.924	3911866	3939909	3994459	4146909	4062239.25	4045929.25	-0.048951118
evm.model.chr9.207	3953634.25	4144295	3925558.75	3997869.5	4121329.75	4084752.75	-0.02149293
evm.model.chr6.998	3977637.25	4023634	4079819.25	4193130	4126490.25	4097607.75	-0.039592459
evm.model.chr7.920	3680325	3629879.25	3767842	4409376	4533302	4527685	-0.282085262
evm.model.chr4.867	4063822.25	4030738.5	4057699.5	4288257.5	4196722.5	4219829	-0.064150015
evm.model.chr11.376	3950103	4204440	4089182.5	4189168	4437499.5	4344319	-0.083245601
evm.model.chr2.503	4247107.5	4361459	4372359	4228412	4201894	4296124.5	0.028565417
evm.model.chr10.99	4073907.5	4082360.75	4095489.25	4534243.5	4601572.5	4562134	-0.160971282
evm.model.chr12.244	4272289	4127162.25	4256764	4474425	4404054.5	4563146.5	-0.086861626

continue on the next page

**Table S2.** continued

Protein	ML-1	ML-2	ML-3	AL-1	AL-2	AL-3	ML vs ML log <sub>2</sub> FC
evm.model.chr4.1133_	4404740.5	4311624	4453310.5	4383902	4383353	4287121.5	0.01268619
evm.model.chr4.1134_							
evm.model.chr5.111	4335035	4211080.5	4242641	4581543	4444855	4461444	-0.076783549
evm.model.Contig841_pilon.2	4264502.5	4050814	4098777.5	4758431.5	4508209	4627230	-0.16246958
evm.model.chr19.223	4338026	4444784.5	4392512.5	4278625	4470196	4455496	-0.003171349
evm.model.chr18.504	4605335	4589092.5	4593564	4555053.5	4423405	4337140.5	0.050294985
evm.model.chr11.439	4595133.5	4516184.5	4384448	4798474	4679351.5	4677698.5	-0.068858291
evm.model.chr18.830	4762787.5	4798936	4736468	4325658.5	4566347	4467844.5	0.09792887
evm.model.chr2.686	4483348	4487775.5	4470883.5	4658723	4851001.5	4811574.5	-0.091413797
evm.model.chr4.2.1	4383161	4304416.5	4232627.5	5100921	5008319	4927043	-0.218819013
evm.model.chr4.647	4697798	4828898.5	4772398.5	4656422	4711746	4736132.5	0.019788723
evm.model.chr6.1152	4421860	4502118	4466790.5	5177243.5	4989258	4969388.5	-0.176734749
evm.model.chr9.143	4705050	4765393	4719219.5	5093093	4966148.5	4987609.5	-0.084621316
evm.model.chr10.600.2	4737645	4767236.5	4762270.5	4840821.5	5115630	5030638.5	-0.071022913
evm.model.chr7.58	4799202.5	4807044.5	4709058.5	5168852.5	5093461	5136100	-0.105223259
evm.model.chr7.117	4910947.5	5097168	5115244	5234417.5	5119022.5	5058202	-0.027241924
evm.model.chr3.280	5075192.5	5204351	5003110.5	5113341	5134052	5021173	0.001330532
evm.model.chr18.601	4824045	4784955	4953015.5	5474169.5	5382582.5	5324659	-0.152127365
evm.model.chr2.32	5067399	5024863	5053050	5184919.5	5343388.5	5204322.5	-0.054888611
evm.model.chr14.470_	4688050	5261941	5287017	5311065	5519771.5	5217002	-0.074799355
evm.model.chr14.471							
evm.model.chr23.321	5114292.5	4941401	4800450.5	5765618.5	5619766	5514555	-0.185958377
evm.model.chr11.792	5498461	5300600	5396359.5	5644268.5	5632447.5	5578985.5	-0.057650744
evm.model.chr9.301	5473078	5673461	5375323	5949777	5977873	5874539.5	-0.107678403
evm.model.chr3.1125	5897430.5	5656997	5462353.5	6021067	5730041	5820051.5	-0.046251243
evm.model.Contig142_pilon.6	5967199.5	5811284	6014650.5	6201156	6196004	6200973.5	-0.063837198
evm.model.chr8.724	5899622	5904930	5835318	6175156.5	6357222.5	6281002	-0.092919214
evm.model.chr4.676	6359346.5	6248294	5895654	6494288	6873307	6657981.5	-0.114061611
evm.model.chr13.443	6431271.5	6420904.5	6490923	6688075.5	6647576	6699619.5	-0.050723073
evm.model.chr1.1123	6852886	6852706.5	6789646	6965906.5	7321035.5	6977491	-0.053153609
evm.model.Contig495_pilon.1	6976384.5	6858472.5	6911679	7130033.5	7244227.5	7284889.5	-0.062106186
evm.model.chr7.153	7088287.5	6862932	7076056	7223085.5	7036103	7134130	-0.024898356
evm.model.chr19.558	7220379	7069391	7305966.5	7232735.5	6951875	6995044.5	0.02806743
evm.model.chr16.92	7415247	7473702	7446770	7330590	7439366	7247658.5	0.020694528
evm.model.chr8.529	6874158.5	6738917	6877109	7894495	8080013.5	7924126	-0.221995214
evm.model.chr16.316.1	7449986	7291709	7161657	7524445	7591582.5	7653828.5	-0.055973497
evm.model.chr16.781	7355649.5	7287324	7318064.5	7814593.5	7929745	7530595	-0.0838308
evm.model.chr22.736	8194517	7935091	7996774	7971483.5	8192796	7981898.5	-0.001183264
evm.model.chr3.388	8051251	8030158	8150649.5	8249731	8142752	8158208	-0.018846665
evm.model.chr4.302	8229641.5	8071775	8045669	8385389.5	8252297.5	7968215	-0.015255321
evm.model.chr9.1020	8163537.5	8437810	8232696	8848085	9281142	9061622	-0.130802017
evm.model.chr23.194	7741119.5	8349371	8114578.5	9493588	9357859	9069341	-0.206030452
evm.model.chr16.357	8537442	8652434	8618188	9780418	9663698	9540396	-0.167460274
evm.model.Contig172_pilon.3	9530170	9546737	9223431	9020934	8822215	9187346	0.066231352
evm.model.chr6.1301	8886516	9237784	9149701	9848900	9842592	9508572	-0.098445177
evm.model.chr17.665	9772007	9506879	9305753	9877496	9803969	9578296	-0.033677915
evm.model.chr12.735	9802641	9732256	9676716	10202170	10136143	10100742	-0.059381547
evm.model.chr23.197	9577819	9497210	9268036	10377133	10623788	10320525	-0.14415504
evm.model.Contig808_pilon.1	9342926	9129339	9407512	15908905	9881583	9832735	-0.353599028

continue on the next page

**Table S2.** continued

Protein	ML-1	ML-2	ML-3	AL-1	AL-2	AL-3	ML vs ML log <sub>2</sub> FC
evm.model.chr1.732	10449492	9891411	9672539	11294056	11268993	11033482	-0.162703496
evm.model.chr10.955	10088197	10462550	10332417	11291354	11394745	11085096	-0.128972665
evm.model.chr14.240	10713036	10507016	10413120	11528456	11542192	11199258	-0.115504006
evm.model.chr22.495	10477604	11523967	10973463	12759140	12565507	12582715	-0.201103915
evm.model.Contig80_pilon.21	12197225	11911762	12078528	13210786	12146773	12930456	-0.081400826
evm.model.chr8.582	13151860	13200450	13223062	13681021	13357976	13195452	-0.023828364
evm.model.chr4.283	15186049	15600704	15384769	13373859	12938018	12925025	0.234792154
evm.model.chr3.1047	13308309	13642998	14207222	15414763	14545526	15042586	-0.128825749
evm.model.chr24.462.7	13803967	13714101	13773811	15371190	15251445	14932030	-0.14174073
evm.model.chr12.512.3	13844135	14162184	14057395	15489006	15411976	14851403	-0.121270713
evm.model.chr7.983	14871351	14621922	14481778	15728209	15555190	15378816	-0.085569541
evm.model.chr6.162.1	14952224	14605692	14396064	17280044	16236462	15645825	-0.161559516
evm.model.chr10.1226	15600046	15409165	14501943	16330992	16647392	15873092	-0.102181984
evm.model.chr11.1260	18113584	17541610	17374280	19848234	19086656	18206382	-0.107738713
evm.model.chr17.363	19742094	18209586	17755790	22932274	22041914	21465778	-0.254180539
evm.model.chr21.78	21881062	21474700	21831870	19775144	19285526	18986608	0.167369852
evm.model.chr9.285	21151614	21163748	20475784	22534582	22710632	22389620	-0.107205327
evm.model.chr18.802	22985662	23192448	22644292	24239850	23251332	23109512	-0.03680412
evm.model.chr4.553	25103346	24948480	25155740	23285596	22598124	23530372	0.115649227
evm.model.chr4.1187	26600258	26265720	26403140	25387144	25797384	24936732	0.058459482
evm.model.chr11.81	30845072	29958190	30164352	34897512	34560080	34320504	-0.190077054
evm.model.chr10.593	34553832	34056688	33896760	39533900	37383284	37635776	-0.160288365
evm.model.chr11.1261	38581828	39170644	38452628	41660660	40973156	39808768	-0.07543201
evm.model.chr4.454	114731944	113730688	111357888	121605840	119714224	117862840	-0.079945712
evm.model.chr4.448	194097536	194264160	190643584	206524560	199080048	194823008	-0.052413829

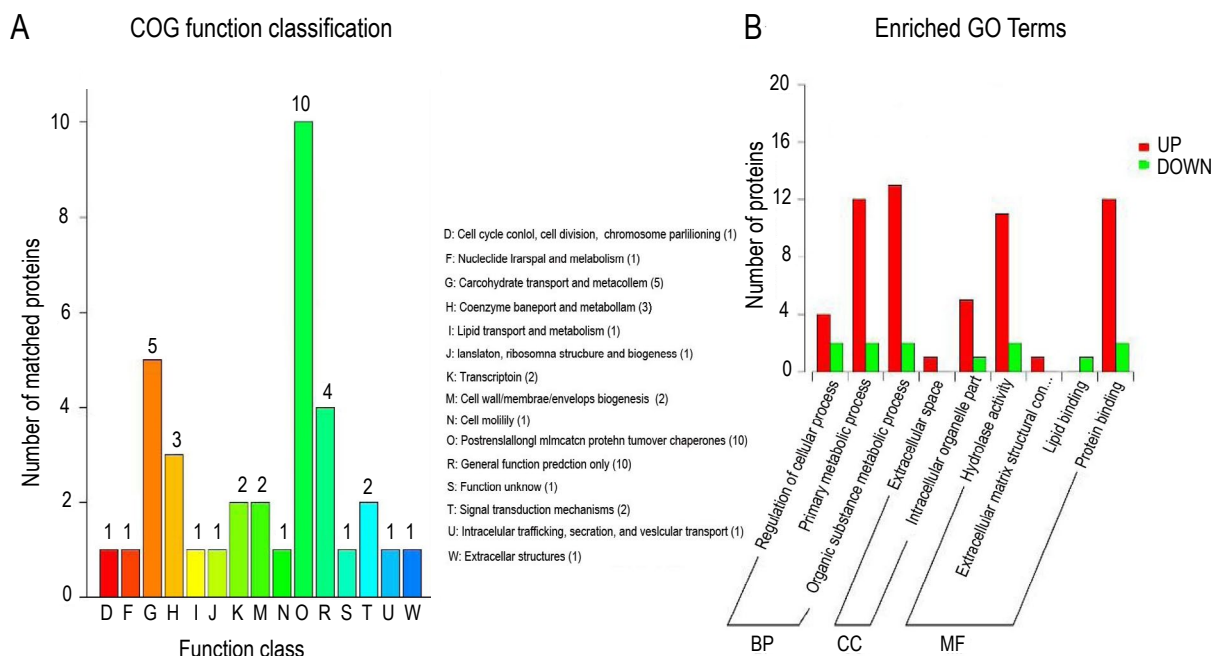


**Figure 4.** Functional annotation of differentially expressed proteins A) function classification of chip on glass (COG) annotation, rainbow bar represents differential classification; B) Gene Ontology (GO) enrichment analysis, red bar depicts the number of over-represented proteins, while green bar represents the number of under-represented proteins; BP – biological process, MF – molecular function, CC – cellular component

transport, and metabolism. For example, 20 DEPs (32% of all DEPs) were associated with transport, metabolism of carbohydrates, coenzymes, lipids, post-translational modifications, protein turnover, and chaperones. DEP functions were characterised by conducting GO enrichment analysis (Jones et al., 2014) (Figure 4B). A total of 63 over-represented GO terms were annotated, and the most significant biological processes (BP) among the up-regulated proteins in ML were related to metabolic processes (primary metabolism) and regulation of cellular processes. GO term: cellular component (CC) was associated with extracellular space and intracellular organelles; the term: molecular function (MF) was related to hydrolase activities, extracellular matrix structural components, and protein binding. The over-represented GO terms among the up-regulated proteins in AL were similar to those assigned to the

up-regulated proteins in ML. However, the expression of several proteins related to extracellular matrix structural components, extracellular space, and lipid binding differed significantly between ML and AL. Moreover, more GO terms have been assigned to the up-regulated proteins in ML than in AL, implying that ML may contribute more to cellular and metabolic processes and hydrolase activities than AL, whereas AL may be more involved in signal transduction and carbohydrate metabolism.

The intracellular pathways affected by DEPs were determined by KEGG analysis. The over-represented KEGG pathways among the up-regulated DEPs in ML were: “pancreatic secretion” and “protein digestion and absorption” (i.e., pathways involved in the digestive system) (Figure 5). Consistent with the high proportion of digestion-related functions of ML proteins, other over-represented



**Figure 5.** Results of Kyoto Encyclopedia of Genes and Genomes (KEGG) enrichment. Scatterplots based on KEGG enrichment of all pathways for significantly differentially expressed proteins (DEPs). Horizontal ratio shows gene numbers of significant DEPs and the total gene number of all annotated genes (pathway entry). Higher ratio value indicates higher degree of enrichment. Multiple hypothesis testing correction was used to determine *q*-value (in the range of 0–1). A *q*-value closer to zero indicates that the enrichment is very high. Items with an up arrow indicate enrichment results for up-regulated proteins; items with a down arrow indicate enrichment results for down-regulated proteins; items with a blank represent enrichment results for up- and down-regulated proteins

KEGG pathways included the downstream “carbohydrate metabolism,” “lipid metabolism,” and “endocrine/excretory system” pathways, reflecting increased energy production required to maintain bodily functions. Furthermore, the enriched KEGG pathways among the up-regulated proteins were related to signal transduction that can regulate cell proliferation, differentiation, apoptosis, and immune responses. The over-represented KEGG pathways among the up-regulated proteins in AL (PXMP4, epithelial splicing regulatory protein 2, isochorismatase, mitochondrial, WIPI3, and ARHG1) were: “peroxisome,” “aminoacyl-tRNA biosynthesis,” “thiamine metabolism,” and “purine metabolism.” Peroxisomes play an important role during the synthesis of bile acids, which are crucial for the absorption of fats and fat-soluble vitamins (e.g., vitamins A and K), which in turn stimulate the metabolism of cofactors and other vitamins (“thiamine metabolism”). In addition, peroxisomes contain oxidative enzymes, including oxidase and uric acid oxidase, which participate in the “aminoacyl-tRNA biosynthesis” and “purine metabolism” KEGG pathways (Yoon et al., 2017). Hence, the digestion-related ML proteins (WD repeat-containing protein 48, protein NDRG1, PDZ and LIM domain protein 1, low choriolytic enzymes, protein S100-A14, protein disulfide-isomerase A2, B2CL1, UBA3, keratin, type II cytoskeletal 8, glyceraldehyde-3-phosphate dehydrogenase 2, alpha-amylase 1, leukocyte elastase inhibitor B, cationic trypsin-3, endoplasmic reticulum resident protein 27, and CEL2A\_2) may be largely responsible for supplying the body with sufficient energy. In contrast, AL peroxisomes may be primarily responsible for the absorption of micronutrients, as well as the metabolism of lipids and nitrogen. The significant abundance of proteins related to vesicles, peroxisomes, lipid binding, Rho GTPase, and antigen processing may provide clues regarding the precise functions of AL. Interestingly, the anatomical position of AL suggests that it may be a gland that can have several liver-related functions (e.g., enzymatic activity, with the joint belt between AL and ML serving as a conduit for enzyme transport), while also supporting immune functions and secreting lipophilic compounds for cold stress adaptation. The location of AL may provide catfish with certain advantages, but this possibility will require experimental verification. Although it is unclear why some catfish species evolved two livers, the phylogenetic diversity revealed by various researchers on the basis of mitochondrial cytochrome b may provide some clues (Yu and He, 2012;

Xiao et al., 2021). An early divergent group among catfish species of the family Sisoridae may have originated from *Pseudocheneis sulcatus*, leading to the formation of two major groups. One group includes genera with AL (e.g., *Exostoma*, *Glaroidoglanis*, and *Glyptosternum*), while the other group consists of genera that may have evolved with only one liver (e.g., *Bagarius* and *Glyptothorax*).

To further clarify the biological functions and mechanisms of action of highly expressed proteins in both ML and AL, Blast2GO was used to identify enriched BP, CC, and MF GO terms (Table S3). The over-represented CC GO terms included those related to ribosomes, intracellular ribonucleoprotein complex, and proteasome complex. Proteins annotated using MF GO terms were associated with oxidoreductase, glutathione transferase, antioxidant, and other catalytic activities. Proteins assigned BP GO terms were related to metabolic, biosynthetic, and catabolic processes, oxygen transport, oxidation-reduction, and lipid metabolism-related activities. KEGG enrichment analysis of these proteins (Table S4) revealed their potential relationships with ribosomes, carbon metabolism, cellular redox homeostasis, fatty acid degradation, glutathione metabolism, and unsaturated fatty acid biosynthesis. The KEGG pathway enrichment analysis of candidate proteins was carried out as previously described. In an earlier study, hypoxia-regulated proteins were identified and used to construct a protein interaction network that indicated that proteins involved in ribosome-related pathways could suppress the translational machinery in cells, thereby conserving energy (Pankaj et al., 2016). In another study conducted to determine the mechanisms mediating fish adaptations to low temperatures, *Oryzias latipes* muscle tissues, acclimated in water at 10 or 30 °C, were collected for RNA-seq analyses, which demonstrated that genes highly expressed at 10 °C were significantly associated with biological processes, including glycolipid metabolic processes and carbon metabolism (Ikeda et al., 2017). Our results suggest that proteins highly expressed in both ML and AL may be involved in *G. maculatum* adaptations to cold and hypoxic conditions. Future studies should focus on these candidate proteins to verify their contribution to the adaptation of *G. maculatum* to high altitudes.

#### Validation of DEPs by PRM analysis

Peptide fragments corresponding to target proteins in different sample groups were used to determine the differences in the expression of target

**Table S3.** Gene Ontology (GO) enrichment analysis of highly expressed proteins in the attached liver and main liver

GO ID	GO Term	GO Class	P-value	Adjusted P-value
GO:1901564	Organonitrogen compound metabolic process	BP	5.18E-34	5.93E-31
GO:1901566	Organonitrogen compound biosynthetic process	BP	8.05E-26	1.84E-23
GO:0034641	Cellular nitrogen compound metabolic process	BP	6.16E-14	2.20E-12
GO:0006807	Nitrogen compound metabolic process	BP	1.68E-15	8.36E-14
GO:0009117	Nucleotide metabolic process	BP	4.55E-11	1.13E-09
GO:0009056	Catabolic process	BP	5.24E-11	1.27E-09
GO:1901575	Organic substance catabolic process	BP	8.40E-11	2.00E-09
GO:0046034	ATP metabolic process	BP	8.63E-11	2.01E-09
GO:0044237	Cellular metabolic process	BP	3.40E-10	7.21E-09
GO:0044712	Single-organism catabolic process	BP	7.33E-10	1.52E-08
GO:0055086	Nucleobase-containing small molecule metabolic process	BP	1.13E-09	2.31E-08
GO:0051186	Cofactor metabolic process	BP	5.54E-09	1.07E-07
GO:0044724	Single-organism carbohydrate catabolic process	BP	8.87E-09	1.61E-07
GO:0044281	Small molecule metabolic process	BP	1.21E-08	2.12E-07
GO:0046496	Nicotinamide nucleotide metabolic process	BP	1.38E-08	2.36E-07
GO:1901135	Carbohydrate derivative metabolic process	BP	4.64E-08	7.58E-07
GO:0071704	Organic substance metabolic process	BP	7.16E-08	1.14E-06
GO:0019637	Organophosphate metabolic process	BP	1.27E-07	1.78E-06
GO:0006082	Organic acid metabolic process	BP	1.28E-07	1.78E-06
GO:0044267	Cellular protein metabolic process	BP	1.32E-07	1.82E-06
GO:0019752	Carboxylic acid metabolic process	BP	7.25E-06	7.33E-05
GO:0005975	Carbohydrate metabolic process	BP	8.60E-07	1.07E-05
GO:0044248	Cellular catabolic process	BP	2.20E-06	2.62E-05
GO:0043436	Oxoacid metabolic process	BP	3.40E-06	3.81E-05
GO:0044238	Primary metabolic process	BP	4.27E-06	4.74E-05
GO:0032787	Monocarboxylic acid metabolic process	BP	4.44E-06	4.88E-05
GO:1901605	Alpha-amino acid metabolic process	BP	0.006188658	0.040653083
GO:0009072	Aromatic amino acid family metabolic process	BP	0.001938878	0.014297659
GO:0044260	Cellular macromolecule metabolic process	BP	0.002161928	0.01573939
GO:0006081	Cellular aldehyde metabolic process	BP	0.003037478	0.021564204
GO:0006006	Glucose metabolic process	BP	0.00514993	0.034223084
GO:0019538	Protein metabolic process	BP	0.000867152	0.006788731
GO:0044282	Small molecule catabolic process	BP	0.000138263	0.001188227
GO:0044723	Single-organism carbohydrate metabolic process	BP	7.71E-06	7.73E-05
GO:0008152	Metabolic process	BP	1.26E-16	7.22E-15
GO:0043603	Cellular amide metabolic process	BP	2.09E-23	3.42E-21
GO:0006518	Peptide metabolic process	BP	4.37E-23	6.25E-21
GO:0019693	Ribose phosphate metabolic process	BP	4.75E-16	2.47E-14
GO:0044710	Single-organism metabolic process	BP	1.07E-12	3.61E-11
GO:0006732	Coenzyme metabolic process	BP	1.09E-11	3.11E-10
GO:0051603	Proteolysis involved in cellular protein catabolic process	BP	0.008385216	0.053246122
GO:1901565	Organonitrogen compound catabolic process	BP	0.008278708	0.053160466
GO:0042157	Lipoprotein metabolic process	BP	0.030151475	0.120080615
GO:0006102	Isocitrate metabolic process	BP	0.021012507	0.090974605
GO:0046128	Purine ribonucleoside metabolic process	BP	1.24E-16	7.22E-15
GO:0072521	Purine-containing compound metabolic process	BP	2.18E-16	1.19E-14
GO:0006163	Purine nucleotide metabolic process	BP	1.63E-14	6.44E-13
GO:0009150	Purine ribonucleotide metabolic process	BP	4.59E-14	1.69E-12
GO:0009205	Purine ribonucleoside triphosphate metabolic process	BP	2.30E-11	5.99E-10
GO:0009167	Purine ribonucleoside monophosphate metabolic process	BP	2.43E-10	5.23E-09
GO:0009206	Purine ribonucleoside triphosphate biosynthetic process	BP	7.18E-07	9.02E-06
GO:0046129	Purine ribonucleoside biosynthetic process	BP	2.91E-06	3.29E-05
GO:0072522	Purine-containing compound biosynthetic process	BP	1.53E-06	1.88E-05
GO:0006164	Purine nucleotide biosynthetic process	BP	6.42E-06	6.67E-05
GO:0009152	Purine ribonucleotide biosynthetic process	BP	1.34E-05	0.00013133

continue on the next page

**Table S3.** continued

GO ID	GO Term	GO Class	P-value	Adjusted P-value
GO:0009168	Purine ribonucleoside monophosphate biosynthetic process	BP	2.69E-05	0.000245868
GO:0044271	Cellular nitrogen compound biosynthetic process	BP	1.08E-20	9.52E-19
GO:0034645	Cellular macromolecule biosynthetic process	BP	3.93E-15	1.80E-13
GO:1901576	Organic substance biosynthetic process	BP	6.50E-15	2.86E-13
GO:0009058	Biosynthetic process	BP	1.09E-16	7.22E-15
GO:0044249	Cellular biosynthetic process	BP	2.58E-15	1.23E-13
GO:0006091	Generation of precursor metabolites and energy	BP	2.36E-05	0.00022274
GO:1901137	Carbohydrate derivative biosynthetic process	BP	0.000209425	0.001773135
GO:0009165	Nucleotide biosynthetic process	BP	0.000534846	0.004245342
GO:0015986	ATP synthesis coupled proton transport	BP	6.40E-06	6.67E-05
GO:0090407	Organophosphate biosynthetic process	BP	0.001548722	0.011645984
GO:0018130	Heterocycle biosynthetic process	BP	0.029496282	0.119131625
GO:0019438	Aromatic compound biosynthetic process	BP	0.01189365	0.069007322
GO:0034654	Nucleobase-containing compound biosynthetic process	BP	0.022308014	0.095390565
GO:0009108	Coenzyme biosynthetic process	BP	0.019917039	0.090974605
GO:0006556	S-adenosylmethionine biosynthetic process	BP	0.021012507	0.090974605
GO:0006096	Glycolytic process	BP	8.00E-08	1.14E-06
GO:0005980	Glycogen catabolic process	BP	0.021012507	0.090974605
GO:0046395	Carboxylic acid catabolic process	BP	0.001004974	0.007814182
GO:0009063	Cellular amino acid catabolic process	BP	0.018878978	0.090974605
GO:0016054	Organic acid catabolic process	BP	5.51E-05	0.000484609
GO:1901606	Alpha-amino acid catabolic process	BP	0.013666513	0.077330815
GO:0009057	Macromolecule catabolic process	BP	0.038107659	0.147152208
GO:0015671	Oxygen transport	BP	0.021012507	0.090974605
GO:0055114	Oxidation-reduction process	BP	5.09E-12	1.49E-10
GO:0045454	Cell redox homeostasis	BP	0.00076873	0.006059711
GO:0006635	Fatty acid beta-oxidation	BP	0.024179424	0.099772857
GO:0006098	Pentose-phosphate shunt	BP	0.021012507	0.090974605
GO:0006412	Translation	BP	9.55E-24	1.82E-21
GO:0006457	Protein folding	BP	3.90E-12	1.17E-10
GO:0009987	Cellular process	BP	6.33E-08	1.02E-06
GO:0010467	Gene expression	BP	2.18E-09	4.38E-08
GO:0006414	Translational elongation	BP	0.00102747	0.007881865
GO:0044699	Single-organism process	BP	0.001284342	0.009721875
GO:0006165	Nucleoside diphosphate phosphorylation	BP	8.87E-09	1.61E-07
GO:0019725	Cellular homeostasis	BP	0.00695881	0.044937398
GO:0098662	Inorganic cation transmembrane transport	BP	0.014012061	0.07818966
GO:0006334	Nucleosome assembly	BP	0.018878978	0.090974605
GO:0006452	Translational frameshifting	BP	0.021012507	0.090974605
GO:0045901	Positive regulation of translational elongation	BP	0.021012507	0.090974605
GO:0045905	Positive regulation of translational termination	BP	0.021012507	0.090974605
GO:0006415	Translational termination	BP	0.024179424	0.099772857
GO:0030168	Platelet activation	BP	0.021012507	0.090974605
GO:0016491	Oxidoreductase activity	MF	2.66E-12	8.68E-11
GO:0016684	Oxidoreductase activity, acting on peroxide as acceptor	MF	0.000514716	0.004205677
GO:0016614	Oxidoreductase activity, acting on CH-OH group of donors	MF	0.00323831	0.022707901
GO:0016702	Oxidoreductase activity, acting on single donors with incorporation of molecular oxygen, incorporation of two atoms of oxygen	MF	0.024179424	0.099772857
GO:0016616	Oxidoreductase activity, acting on the CH-OH group of donors, NAD or NADP as acceptor	MF	0.009101512	0.055631164
GO:0004364	Glutathione transferase activity	MF	0.003037478	0.021564204
GO:0016209	Antioxidant activity	MF	0.001129831	0.008609313
GO:0005198	Structural molecule activity	MF	1.08E-31	6.17E-29
GO:0003735	Structural constituent of ribosome	MF	3.01E-31	1.15E-28
GO:0051082	Unfolded protein binding	MF	1.71E-07	2.32E-06

continue on the next page

**Table S3.** continued

GO ID	GO Term	GO Class	P-value	Adjusted P-value
GO:0004298	Threonine-type endopeptidase activity	MF	2.23E-05	0.000212846
GO:0016829	Lyase activity	MF	0.000379615	0.003190441
GO:0003746	Translation elongation factor activity	MF	0.00102747	0.007881865
GO:0004332	Fructose-bisphosphate aldolase activity	MF	0.001938878	0.014297659
GO:0051920	Peroxiredoxin activity	MF	0.001938878	0.014297659
GO:0008184	Glycogen phosphorylase activity	MF	0.003037478	0.021564204
GO:0043168	Anion binding	MF	0.003106882	0.021920781
GO:0016758	Transferase activity, transferring hexosyl groups	MF	0.004513082	0.031453977
GO:0005200	Structural constituent of cytoskeleton	MF	0.004788356	0.032772998
GO:0016765	Transferase activity, transferring alkyl or aryl (other than methyl) groups	MF	0.004788356	0.032772998
GO:0005544	Calcium-dependent phospholipid binding	MF	0.00514993	0.034223084
GO:0019843	rRNA binding	MF	0.00514993	0.034223084
GO:0015078	Hydrogen ion transmembrane transporter activity	MF	0.009101512	0.055631164
GO:0030170	Pyridoxal phosphate binding	MF	0.009101512	0.055631164
GO:0008483	Transaminase activity	MF	0.010646545	0.0631863
GO:0003824	Catalytic activity	MF	0.014198223	0.078779458
GO:0004743	Pyruvate kinase activity	MF	0.021012507	0.090974605
GO:0030955	Potassium ion binding	MF	0.021012507	0.090974605
GO:0004618	Phosphoglycerate kinase activity	MF	0.021012507	0.090974605
GO:0004134	4-alpha-glucano transferase activity	MF	0.021012507	0.090974605
GO:0004135	Amylo-alpha-1,6-glucosidase activity	MF	0.021012507	0.090974605
GO:0004450	Isocitrate dehydrogenase (NADP <sup>+</sup> ) activity	MF	0.021012507	0.090974605
GO:0004478	Methionine adenosyl transferase activity	MF	0.021012507	0.090974605
GO:0004634	Phosphopyruvate hydratase activity	MF	0.021012507	0.090974605
GO:0042132	Fructose 1,6-bisphosphate 1-phosphatase activity	MF	0.021012507	0.090974605
GO:0016830	Carbon-carbon lyase activity	MF	0.027109836	0.110666222
GO:0016836	Hydro-lyase activity	MF	0.030151475	0.120080615
GO:0019205	Nucleobase-containing compound kinase activity	MF	0.044621206	0.167769862
GO:0005840	Ribosome	CC	1.14E-30	3.25E-28
GO:0030529	Intracellular ribonucleoprotein complex	CC	5.30E-21	5.04E-19
GO:0043232	Intracellular non-membrane-bounded organelle	CC	1.14E-18	8.68E-17
GO:0044444	Cytoplasmic part	CC	7.33E-15	3.10E-13
GO:0005737	Cytoplasm	CC	8.79E-13	3.04E-11
GO:0032991	Macromolecular complex	CC	1.06E-08	1.89E-07
GO:0044424	Intracellular part	CC	2.85E-07	3.83E-06
GO:0005622	Intracellular	CC	5.60E-07	7.36E-06
GO:0043229	Intracellular organelle	CC	1.79E-06	2.15E-05
GO:0000786	Nucleosome	CC	6.40E-06	6.67E-05
GO:0044464	Cell part	CC	6.80E-06	6.94E-05
GO:0005839	Proteasome core complex	CC	2.23E-05	0.000212846
GO:1905368	Peptidase complex	CC	3.74E-05	0.000339005
GO:0000502	Proteasome complex	CC	4.98E-05	0.000444548
GO:0099513	Polymeric cytoskeletal fiber	CC	0.00052249	0.004205677
GO:0005874	Microtubule	CC	0.004788356	0.032772998
GO:0044445	Cytosolic part	CC	0.00514993	0.034223084
GO:0030660	Golgi-associated vesicle membrane	CC	0.010646545	0.0631863
GO:0030126	COPI vesicle coat	CC	0.010835096	0.0631863
GO:0015934	Large ribosomal subunit	CC	0.010835096	0.0631863
GO:1902494	Catalytic complex	CC	0.013293116	0.075592195
GO:0005882	Intermediate filament	CC	0.019917039	0.090974605
GO:0008250	Oligosaccharyltransferase complex	CC	0.021012507	0.090974605
GO:0005577	Fibrinogen complex	CC	0.021012507	0.090974605
GO:0000015	Phosphopyruvate hydratase complex	CC	0.021012507	0.090974605
GO:0005833	Hemoglobin complex	CC	0.021012507	0.090974605
GO:0005764	Lysosome	CC	0.030151475	0.120080615
GO:0005783	Endoplasmic reticulum	CC	0.045027522	0.168742484

BP – biological process, MF – molecular function, CC – cellular component

**Table S4.** Kyoto Encyclopedia of Genes and Genomes enrichment analysis of highly expressed proteins in the attached liver and main liver

MapID	MapTitle	P-value	Adjusted P-value
Map03010	Ribosome	1.56E-31	4.42E-29
Map01200	Carbon metabolism	3.20E-13	3.46E-11
Map01230	Biosynthesis of amino acids	3.67E-13	3.46E-11
Map00010	Glycolysis/Gluconeogenesis	3.71E-12	2.63E-10
Map00680	Methane metabolism	3.56E-08	2.01E-06
Map00710	Carbon fixation in photosynthetic organisms	9.99E-08	4.71E-06
Map00260	Glycine, serine and threonine metabolism	6.09E-07	2.46E-05
Map00980	Metabolism of xenobiotics by cytochrome P450	1.28E-05	0.000422409
Map00330	Arginine and proline metabolism	1.34E-05	0.000422409
Map05204	Chemical carcinogenesis	2.34E-05	0.000662774
Map00982	Drug metabolism – cytochrome P450	4.20E-05	0.001079768
Map00380	Tryptophan metabolism	0.000188466	0.00444466
Map00020	Citrate cycle (TCA cycle)	0.000229952	0.005005878
Map00071	Fatty acid degradation	0.000370186	0.007242644
Map00030	Pentose phosphate pathway	0.000402751	0.007242644
Map00620	Pyruvate metabolism	0.000409478	0.007242644
Map00630	Glyoxylate and dicarboxylate metabolism	0.00052876	0.008493579
Map00625	Chloroalkane and chloroalkene degradation	0.000540228	0.008493579
Map00410	beta-Alanine metabolism	0.000593815	0.008844723
Map00270	Cysteine and methionine metabolism	0.001301532	0.018416677
Map00480	Glutathione metabolism	0.001420364	0.018946375
Map00053	Ascorbate and aldarate metabolism	0.001593137	0.018946375
Map00340	Histidine metabolism	0.001593137	0.018946375
Map00670	One carbon pool by folate	0.00160676	0.018946375
Map00280	Valine, leucine and isoleucine degradation	0.002312217	0.025611682
Map01210	2-Oxocarboxylic acid metabolism	0.002353017	0.025611682
Map00350	Tyrosine metabolism	0.002709268	0.028397141
Map04612	Antigen processing and presentation	0.00286962	0.029003657
Map05134	Legionellosis	0.003862359	0.037691297
Map04512	ECM-receptor interaction	0.004324885	0.040798077
Map00626	Naphthalene degradation	0.005190472	0.047383989
Map03320	PPAR signaling pathway	0.005658808	0.050045083
Map04141	Protein processing in endoplasmic reticulum	0.007582974	0.065029744
Map01220	Degradation of aromatic compounds	0.009995973	0.080824582
Map00310	Lysine degradation	0.014511017	0.114072718
Map00250	Alanine, aspartate and glutamate metabolism	0.01704768	0.130391715
Map00400	Phenylalanine, tyrosine and tryptophan biosynthesis	0.01807554	0.134615209
Map04918	Thyroid hormone synthesis	0.019169025	0.139098313
Map00040	Pentose and glucuronate interconversions	0.024870001	0.164416581
Map00051	Fructose and mannose metabolism	0.024870001	0.164416581
Map05322	Systemic lupus erythematosus	0.026272154	0.168977715
Map00643	Styrene degradation	0.030032208	0.188869222
Map00720	Carbon fixation pathways in prokaryotes	0.032400025	0.190930371
Map04964	Proximal tubule bicarbonate reclamation	0.032400025	0.190930371
Map00830	Retinol metabolism	0.033733281	0.190930371
Map01040	Biosynthesis of unsaturated fatty acids	0.033733281	0.190930371
Map00500	Starch and sucrose metabolism	0.035891845	0.199164551
Map00903	Limonene and pinene degradation	0.039398187	0.214417057
Map00360	Phenylalanine metabolism	0.042075136	0.220504877

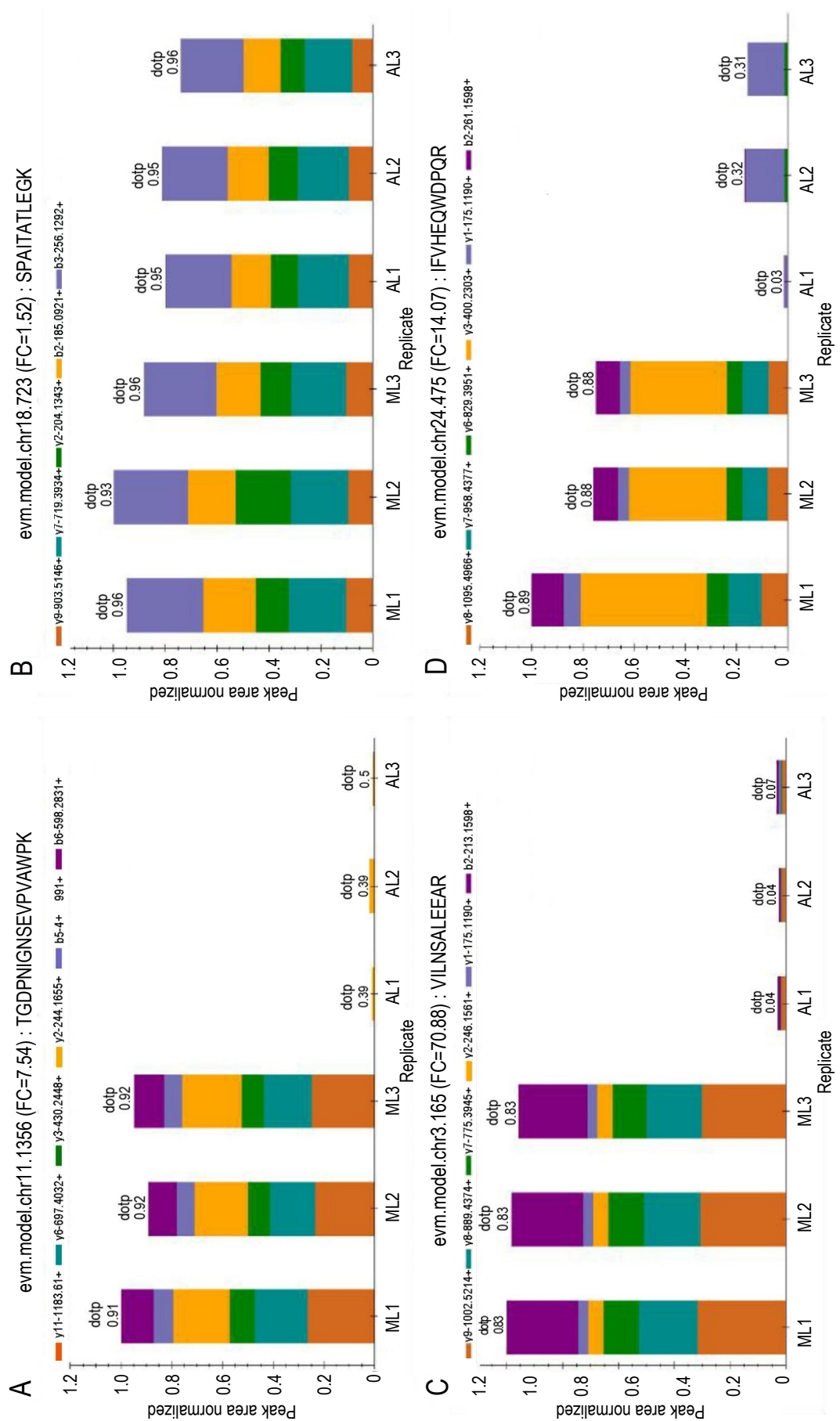


**Figure 6.** Bar plots created using Skyline illustrate the peak area (shown for triplicate analyses) for 4 target proteins. Colour-coded bars represent the involvement of each individual transition to the total peak area and match the colour scheme in the transition panel, data in brackets indicate fold change of main liver/attached liver (ML/AL) in data-independent acquisition analysis liver

proteins related to lipid metabolism, ATP-binding, hormone and serine-type endopeptidase activities among the sample groups. Quantitative data for target peptide fragments were obtained for all six samples based on LC-PRM/MS analysis conducted using four peptide fragments from four target proteins in two groups of liver samples (Figure 6). The heavy isotope-labelled peptide fragments were used for subsequent relative quantitative analysis. The results indicated that the expression levels of three target proteins associated with lipid metabolism, hormone activities, and serine-type endopeptidase activities in the ML group were significantly higher compared to the expression of the protein related to ATP-binding in the AL group. The expression level of one target protein associated with hormone activities was slightly higher in the ML group than in the AL group, which was consistent with the DIA data. This confirmed the results for several proteins that were significantly modulated in the two livers. To the best of our knowledge, this study is the first to use LC-PRM to analyse the catfish liver proteome. Therefore, the methods used in this study may be relevant for future research on specific catfish liver proteins or biomarkers.

## Discussion

Adverse weather conditions have limited the distribution of living organisms due to their effects on physiological functions and the integrity of cellular structures (Aberle et al., 2020). Diverse glyptosternoid species in the rivers of the Tibetan Plateau and their tributaries have adapted to high-altitude conditions, making them ideal model organisms for examining the genetic basis of adaptations to high altitudes. The physiological status of *G. maculatum* may be efficiently evaluated by analysing the haematological system, including blood biochemical characteristics (Altinok-Yipel et al., 2022). However, other cyprinid and cobitid fish species, such as *Bagarius bagarius* (Hamilton), *Glyptothorax sinensis* (Regan), and *Glyptothorax fukiensis* lack AL, but can still survive at high altitudes (Cox et al., 2014). Therefore, altitude may not be the only factor that have contributed to the formation of the second liver in *G. maculatum*. A major challenge for species at high elevations is coping with low oxygen supply (Beall, 2007).

One of the objectives of this study was to functionally characterise DEPs in AL. After processing the generated data, 63 DEPs were identified in DIA MS analysis and subsequently validated using

PRM, COG, GO, and KEGG analyses revealed that the detected DEPs belonged to 15 functional categories. A significant proportion of the upregulated DEPs could be annotated with BP GO terms (e.g., regulation of cellular process, primary metabolic process, and organic substance metabolic process), CC GO terms (e.g., extracellular space and intracellular organelle) or MF GO terms (e.g., hydrolase activity, extracellular matrix structural constituent, and protein binding). Moreover, the identified DEPs included muscle myosin heavy chain 6 alpha, Cu/Zn superoxide dismutase, cytochrome c oxidase, NADH dehydrogenase, ATP synthase, catalase, manganese superoxide dismutase, chymotrypsin-like elastase family member 2A isoform 4, PXMP4, and ARHG1, as well as proteins associated with aminoacetyl-tRNA, thiamine metabolism, and purine metabolism.

Many AL-related proteins have been predicted to be involved in the micronutrient absorption (e.g., peroxisomal enzymes and oxidative enzymes), lipid binding, and antigenic processing that affect multiple liver functions, including bile production and excretion, hormone excretion, metabolism (fats, proteins, and carbohydrates), enzyme activation, storage (glycogen, vitamins, and minerals), synthesis of plasma proteins (clotting factors), as well as blood detoxification and purification. In addition to proteins related to aminoacetyl-tRNA, thiamine metabolism and purine metabolism, AL DEPs also included PXMP4 and ARHG1. Peroxisome-related proteins (e.g., PXMP4) and hypoxia-inducible factors (HIFs) affect many signalling pathways involved in physiological stress responses and induce the expression of hypoxia-responsive genes. Additionally, HIFs are post-translationally regulated by the following members of the O<sub>2</sub>-dependent HIF hydroxylase family: four prolyl 4-hydroxylases and an asparaginyl hydroxylase. These enzymes are abundant in the resting liver, which has a unique physiological O<sub>2</sub> gradient (He et al., 2021). Earlier research demonstrated that HIFs and their regulatory hydroxylases in primary rat hepatocytes cultured under hypoxia-reoxygenation conditions were located in peroxisomes. Furthermore, HIF hydroxylases translocate from the nucleus to the cytoplasm under hypoxic conditions, but accumulate in peroxisomes in response to reoxygenation. Thus, peroxisomes are critical for the endogenous HIF pathway in hepatocytes (Khan et al., 2006).

A hypoxia resistance-related gene encoding arginyl-tRNA synthetase, which is essential for protein translation, protects *Caenorhabditis elegans*

from hypoxia-induced death, with an inverse correlation between hypoxia resistance and translation rate (Anderson et al., 2009). Thiamine deficiency activates HIF-1 $\alpha$  to mediate pro-apoptotic responses in mouse primary astrocytes. Consistent with the effects of hypoxia/ischemia, thiamine deficiency stabilises and activates HIF-1 $\alpha$  under physiological oxygen levels. Induction of HIF-1 $\alpha$ -mediated transcriptional up-regulation of pro-apoptotic signalling pathways contributes to astrocyte cell death in thiamine-deficient environments (Zera et al., 2017). Furthermore, HIF-1 $\alpha$  was shown to play a major role in the hypoxia-inducible expression of the thiamine transporter gene *SLC19A3* (Zera et al., 2016). An earlier study investigated purine metabolism in erythrocytes and plasma of bottlenose dolphins (*Tursiops truncatus*) exposed to hypoxic conditions induced by breath-hold diving and exercise (Velasco-Martínez et al., 2016). Hypoxia modulated the purine salvage pathway and decreased red blood cell and supernatant hypoxanthine levels at low temperatures (Nemkov et al., 2018). Guanine nucleotide exchange factors (GEFs) are proteins or protein domains involved in the activation of small GTPases, which are active when bound to GTP, while inactive when bound to GDP. Hence, GTPase activities are regulated by GEFs, as well as by GTPase-activating proteins (Hashim and Mokhtar, 2021). A total of 63 fast-evolving genes (FEGs) and 48 positively selected genes (PSGs) have been previously identified in *G. maculatum*, which differed in comparison to 121–178 FEGs and 58–244 PSGs detected in other living glyptosternoid fish species (Cox et al., 2014). Functional enrichment analysis indicated that FEGs in *G. maculatum* generally encoded proteins related to structural components. The identification of candidate PSGs in *G. maculatum*, which may directly contribute to adaptive responses to high altitude (Zhang et al., 2021), in combination with *G. maculatum* draft genome sequence, may help characterise the DEPs detected in the current study.

The following candidate PSGs have been identified in glyptosternoids and may be responsive to hypoxic conditions: *Slc2a8*, *Igfbp7*, *C2*, *Cp*, *Ndc1*, *Hspa5*, *Ttr*, *Gapdh*, *Prmt5*, *Srebfl*, *Perp*, *Map3k14*, and *Fam162a*. These genes are significantly associated with energy metabolism and oxidation functions (e.g., “ATP binding,” “mitochondrial part,” “GTPase regulator activity,” “ATPase activity,” and “acyl-CoA oxidase/dehydrogenase”). The genes are most likely involved in the adaptation to high altitudes, especially those associated with response to hypoxia and oxygen binding. For example, solute

carrier family 2 (facilitated glucose transporter) member 8 belongs to the solute carrier 2A family, which includes intracellular glucose transporters regulated by HIF-1 $\alpha$  (Saxena et al., 2007; Shao et al., 2014). Other proteins, including antioxidant enzymes like superoxide dismutase, cellular retinol-binding protein, and glutathione-S-transferase, as well as chaperone HSP60 and protein disulphide isomerase are reportedly involved in adaptive processes in *Carcinus maenas* (Nassereddine et al., 2021), *Nucella lapillus* (Cunha et al., 2007), and *Clarias gariepinus* (Saliu and Bawa-Allah, 2012).

Genes encoding proteins affecting developmental processes were frequently assigned mechanisms underlying responses to hypoxia and energy metabolism. Mitochondria are crucial for ATP production and heat generation, and intense selection pressure may preferentially affect mitochondria at high altitudes (Birrell et al., 2020). Cytochrome c oxidase is a mitochondrial enzyme that reduces  $\text{NO}_2^-$  to NO, which induces the expression of genes associated with the nuclear hypoxia response, possibly through a pathway that involves protein nitration (Castello et al., 2006). Thus, modification of the structure and/or activity of cytochrome c oxidase or complex IV of the respiratory chain may contribute to adaptation to hypoxic environments. However, it remains unclear how other fish species without AL can survive under similar environmental conditions. Owing to the fact that distinct functions of AL proteins related to adaptation to environmental conditions (e.g., those at high altitudes) have not been identified, one must consider the possibility that AL and ML proteins interact to optimally coordinate physiological processes. Moreover, all organisms exhibit unique responses to different stimuli. To the best of our knowledge, our study is the first to complete a thorough comparative analysis of the ML and AL proteomes. Although the involvement of AL in vitamin absorption and amino acid metabolism has been elucidated, future studies will need to determine how these AL functions contribute to the adaptation of *G. maculatum* to environmental stresses.

Under hypoxic conditions, cellular ATP levels decrease due to degradation of purine nucleotides (Akiyama et al., 2022). The purine salvage pathway is critical for maintaining the nucleotide pool and *de novo* ATP synthesis (Davis et al., 2004). Our GO enrichment analysis identified 28 proteins involved in purine metabolism processes, suggesting that they may play prominent roles during ATP synthesis in *G. maculatum*. Several catabolic processes may also help maintain cellular homeostasis and facil-

tate adaptations to low-oxygen stress. For example, glycolysis is a conserved metabolic pathway that converts glucose into pyruvate, while releasing free energy as ATP under hypoxia (Tran et al., 2016). GO and KEGG pathway analyses showed that 30 highly expressed proteins were involved in glycolytic processes, including in liver cells, generating energy under low-oxygen conditions (Yang et al., 2021). This phenomenon has also been observed in previous studies. More specifically, the level of glycolytic enzymes in the cortex and hippocampus was shown to increase in order to produce the energy required for survival after short-term exposure to hypobaric hypoxia (Sharma et al., 2013).

Other plateau-adapted oxygen transport proteins (GO:0015671) may also play important roles under hypoxic conditions. The *EPAS1* gene encodes an oxygen transport protein involved in the HIF pathway; this protein likely affects the adaptation of humans and other animals to high altitudes (Pan et al., 2017). In the current study, two highly expressed proteins related to oxygen transport have been identified. The molecular functions of these two proteins needs to be verified.

Fatty acid synthesis can protect cells from the adverse effects of extreme conditions in the Tibetan plateau (Murray et al., 2018). Hypoxia induces an increase in fatty acid levels in various tissues, probably because of a decrease in lipid oxidation or an increase in lipid contents (Usman et al., 2022). Previous studies have indicated that elevated fatty acid biosynthesis from Gln/Glu, followed by an esterification, may be a neuronal specific pathway for hypoxia adaptation (Brose et al., 2014). Before Gln can be used for fatty acid synthesis, it must be converted to Glu by glutaminase and due to this additional step, Glu may be a better substrate (Agrawal et al., 2020). Compartmentalisation of Glu and Gln metabolism prevents mixing of the Glu and Gln product pools. Each substrate can be channelled to fatty acid synthesis through different enzymatic systems at different rates (McKenna et al., 2000). In our GO analysis, two groups of proteins were assigned BP GO terms “lipoprotein metabolic process” (GO:0042157) and “fatty acid beta-oxidation” (GO:0006635). KEGG pathway analysis revealed 10 proteins associated with “alanine, aspartate and glutamate metabolism” (MapID:map00250), whereas seven proteins were related to “biosynthesis of unsaturated fatty acids” (MapID:map01040). It remains to be verified whether the molecular mechanisms underlying the effects of these proteins on adaptive responses to hypoxic conditions are consistent with previous studies.

In this study, ribosome-related proteins were significantly enriched, which was consistent with the results of earlier research (Shah et al., 2011). Since organisms can conserve energy by suppressing protein synthesis, modifying ribosomal functions is an effective way to minimize hypoxia-induced protein changes and confer hypoxia tolerance (Gerasimovskaya et al., 2005). In a previous study, deletion of five genes significantly increased hypoxia tolerance. All of these genes encode proteins involved in ribosome biogenesis. Subsequent analysis of deletion mutants showed that silencing these genes minimized hypoxia-induced changes in polyribosome profiles and protein synthesis.

## Conclusions

The present study provided useful information on the basis of a comparative analysis of proteomic data obtained for ML and AL in *G. maculatum*. The distinct role of AL (i.e., vitamin absorption and nitrogen metabolism) was determined, but the evolutionary benefit of AL needs to be further investigated. Nevertheless, the high peroxisomal and tubulin-related activities in AL suggest that it may function as a sebaceous gland in adaptive responses to cold conditions. Unfortunately, we were unable to formulate a viable hypothesis regarding the involvement of AL in adaptive evolution. Future studies should investigate AL in other related catfish species, and compare catfish species containing ML and AL with those that only possess ML. Information gained over the past few years from the available draft genome sequence, liver transcriptome and proteome data (this study) make *G. maculatum* an indispensable resource for studying catfish adaptations to high-altitude environments.

## Funding source

This work was supported by the Key Research and Development Projects in Tibet (No. ZH20200002), Key Research and Development Projects in Anhui (No. 201904e01020008), Key Research and Development Projects in Tibet (No. XZ202001ZY0040N), Anhui Province Foundation for Talent in Higher Education (No. jxbjZD22), Anhui Polytechnic University Scientific Research Starting Foundation for the Introduction of Talent (No. 2018YQQ011), Anhui Polytechnic University Young and Middle-aged Talents Project (No. 2018-2019), High Level Talent Introduction Project (No. 2018PTJB03), Talent Introduction Project of Hefei

Normal University (No. 403-60420050) and Qinghai Provincial Key Laboratory of Physical Geography and Environmental Process, Qinghai Provincial Innovation Platform Construction Special Project (No. 2020-ZJ-Y06)

## Conflict of interest

The Authors declare that there is no conflict of interest.

## References

- Aberle L., Kruger A., Reber J.M. et al., 2020. PARP1 catalytic variants reveal branching and chain length-specific functions of poly (ADP-ribose) in cellular physiology and stress response. *Nucleic Acids Res.* 48, 10015–10033, <https://doi.org/10.1093/nar/gkaa590>
- Agrawal S., Karcher D., Ruf S., Bock R., 2020. The functions of chloroplast glutamyl-tRNA in translation and tetrapyrrole biosynthesis. *Plant Physiol.* 183, 263–276, <https://doi.org/10.1104/pp.20.00009>
- Akiyama M., Mizokami T., Miyamoto S., Ikeda Y., 2022. Kaempferol increases intracellular ATP content in C2C12 myotubes under hypoxic conditions by suppressing the HIF-1α stabilization and/or by enhancing the mitochondrial complex IV activity. *J. Nutr. Biochem.* 103, 108949, <https://doi.org/10.1016/j.jnutbio.2022.108949>
- Altinok-Yipel F., Yipel M., Altug N., Ozdemir N., 2022. Blood concentrations of potentially toxic trace elements (PTEs) and correlation with biochemical and hematological parameters in dogs from thrace region, Turkey. *Chemosphere* 293, 133649, <https://doi.org/10.1016/j.chemosphere.2022.133649>
- Anderson L.L., Mao X., Scott B.A., Crowder C.M., 2009. Survival from hypoxia in *C. elegans* by inactivation of aminoacyl-tRNA synthetases. *Science* 323, 630–633, <https://doi.org/10.1126/science.1166175>
- Anjo S.I., Santa C., Manadas B., 2017. SWATH-MS as a tool for biomarker discovery: from basic research to clinical applications. *Proteomics* 17, 1600278, <https://doi.org/10.1002/pmic.201600278>
- Beall C.M., 2007. Two routes to functional adaptation: Tibetan and Andean high-altitude natives. *Proc. Natl. Acad. Sci. U.S.A.* 104, 8655–8660, <https://doi.org/10.1073/pnas.0701985104>
- Birrell J.H., Shah A.A., Hotaling S., Giersch J.J., Williamson C.E., Jacobsen D., Woods H.A., 2020. Insects in high-elevation streams: life in extreme environments imperiled by climate change. *Glob. Change Biol.* 26, 1–18, <https://doi.org/10.1111/gcb.15356>
- Brose S.A., Marquardt A.L., Golovko M.Y., 2014. Fatty acid biosynthesis from glutamate and glutamine is specifically induced in neuronal cells under hypoxia. *J. Neurochem.* 129, 400–412, <https://doi.org/10.1111/jnc.12617>
- Bruderer R., Bernhardt O.M., Gandhi T. et al., 2015. Extending the limits of quantitative proteome profiling with data-independent acquisition and application to acetaminophen-treated three-dimensional liver microtissues. *Mol. Cell. Proteomics* 14, 1400–1410, <https://doi.org/10.1074/mcp.M114.044305>
- Castello P.R., David P.S., McClure T., Crook Z., Poyton R.O., 2006. Mitochondrial cytochrome oxidase produces nitric oxide under hypoxic conditions: implications for oxygen sensing and hypoxic signaling in eukaryotes. *Cell Metab.* 3, 277–287, <https://doi.org/10.1016/j.cmet.2006.02.011>
- Cox J., Hein M.Y., Luber C.A., Paron I., Nagaraj N., Mann M., 2014. Accurate proteome-wide label-free quantification by delayed normalization and maximal peptide ratio extraction, termed MaxLFQ. *Mol. Cell. Proteomics* 13, 2513–2526, <https://doi.org/10.1074/mcp.M113.031591>
- Cunha I., Mangas-Ramirez E., Guilhermino L., 2007. Effects of copper and cadmium on cholinesterase and glutathione S-transferase activities of two marine gastropods (*Monodonta lineata* and *Nucella lapillus*). *Comp. Biochem. Physiol. C Toxicol. Pharmacol.* 145, 648–657, <https://doi.org/10.1016/j.cbpc.2007.02.014>
- Davis R.W., Polasek L., Watson R., Fuson A., Williams T.M., Kanato S.B., 2004. The diving paradox: new insights into the role of the dive response in air-breathing vertebrates. *Comp. Biochem. Phys. A Mol. Integr. Physiol.* 138, 263–268, <https://doi.org/10.1016/j.cbpb.2004.05.003>
- Dietrich M., Judycka S., Żarski D., Malinowska A., Świderska B., Palinińska-Żarska K., Błażejewski M., Ciereszko A., 2021. Proteomic analysis of pikeperch seminal plasma provides novel insight into the testicular development of domesticated fish stocks. *Animal* 15, 100279, <https://doi.org/10.1016/j.animal.2021.100279>
- Gerasimovskaya E.V., Tucker D.A., Stenmark K.R., 2005. Activation of phosphatidylinositol 3-kinase, Akt, and mammalian target of rapamycin is necessary for hypoxia-induced pulmonary artery adventitial fibroblast proliferation. *J. Appl. Physiol.* 98, 722–735, <https://doi.org/10.1152/japplphysiol.00715.2004>
- Goeminne L.J.E., Gevaert K., Clement L., 2018. Experimental design and data-analysis in label-free quantitative LC/MS proteomics: a tutorial with MSqRob. *J. Proteomics* 171, 23–36, <https://doi.org/10.1016/j.jprot.2017.04.004>
- Han X., Chen L., Hu Z., Chen L., Sun P., Wang Y., Liu Y., 2021. Identification of proteins related with pemetrexed resistance by iTRAQ and PRM-based comparative proteomic analysis and exploration of IGF2BP2 and FOLR1 functions in non-small cell lung cancer cells. *J. Proteomics* 237, 104122, <https://doi.org/10.1016/j.jprot.2021.104122>
- Hashim I.F., Mokhtar A.M.A., 2021. Small Rho GTPases and their associated RhoGEFs mutations promote immunological defects in primary immunodeficiencies. *Int. J. Biochem. Cell Biol.* 137, 106034, <https://doi.org/10.1016/j.biocel.2021.106034>
- He W., Batty-Stuart S., Lee J.E., Ohh M., 2021. HIF-1α hydroxyprolines modulate oxygen-dependent protein stability via single VHL interface with comparable effect on ubiquitination rate. *J. Mol. Biol.* 433, 167244, <https://doi.org/10.1016/j.jmb.2021.167244>
- Huijuan Z., 2011. Genesis of liver in *Glyptosternon maculatum* and related bioadaptive studies, in Library of Huazhong Agricultural University. Huazhong Agricultural University. Wuhan, HB (China)
- Ikeda D., Koyama H., Mizusawa N., Kan-No N., Tan E., Asakawa S., Watabe S., 2017. Global gene expression analysis of the muscle tissues of medaka acclimated to low and high environmental temperatures. *Comp. Biochem. Physiol. Part D. Genomics Proteomics* 24, 19–28, <https://doi.org/10.1016/j.cbd.2017.07.002>
- Jones P., Binns D., Chang H.Y. et al., 2014. InterProScan 5: genome-scale protein function classification. *Bioinformatics* 30, 1236–1240, <https://doi.org/10.1093/bioinformatics/btu031>
- Kelstrup C.D., Bekker-Jensen D.B., Arrey T.N., Hogrebe A., Harder A., Olsen J.V., 2017. Performance evaluation of the Q exactive HF-X for shotgun proteomics. *J. Proteome Res.* 17, 727–738, <https://doi.org/10.1021/acs.jproteome.7b00602>
- Kelstrup C.D., Young C., Lavallee R., Nielsen M.L., Olsen J.V., 2012. Optimized fast and sensitive acquisition methods for shotgun proteomics on a quadrupole orbitrap mass spectrometer. *J. Proteome. Res.* 11, 3487–3497, <https://doi.org/10.1021/pr3000249>

- Khan Z., Michalopoulos G.K., Stoltz D.B., 2006. Peroxisomal localization of hypoxia-inducible factors and hypoxia-inducible factor regulatory hydroxylases in primary rat hepatocytes exposed to hypoxia-reoxygenation. *Am. J. Pathol.* 169, 1251–1269, <https://doi.org/10.2353/ajpath.2006.060360>
- Khramtsov P., Kalashnikova T., Bochkova M., Kropaneva M., Timanova S., Rayev M., 2021. Measuring the concentration of protein nanoparticles synthesized by desolvation method: comparison of Bradford assay, BCA assay, hydrolysis/UV spectroscopy and gravimetric analysis. *Int. J. Pharm.* 599, 120422, <https://doi.org/10.1016/j.ijpharm.2021.120422>
- Li H., Xie X., Li D., Chai Y., Liu H., Fan Q., Zhu B., 2017. Exo-celiac Liever in *Glyptosternon maculatum*. *Prog. Nat. Sci.* 17, 1109–1113
- Li Y., Burridge C.P., Lv Y., Peng Z., 2021. Morphometric and population genomic evidence for species divergence in the *Chimarrichthys* fish complex of the Tibetan Plateau. *Mol. Phylogenet. Evol.* 159, 107117, <https://doi.org/10.1016/j.ympev.2021.107117>
- Liao X., Pan Q., Tian X., Wu X., Zhao F., 2022. Proteomic analysis of the electron uptake pathway of *Rhodopseudomonas palustris* CGA009 under different cathodic potentials. *Process Biochem.* 115, 42–48, <https://doi.org/10.1016/j.procbio.2022.01.026>
- Liu H., Liu Q., Chen Z. et al., 2018. Draft genome of *Glyptosternon maculatum*, an endemic fish from Tibet Plateau. *Gigascience* 7, giy104, <https://doi.org/10.1093/gigascience/giy104>
- Ma X., Dai W., Kang J., Yang L., He S., 2016. Comprehensive transcriptome analysis of six catfish species from an altitude gradient reveals adaptive evolution in Tibetan fishes. *G3-Genes Genom. Genet.* 6, 141–148, <https://doi.org/10.1534/g3.115.024448>
- McKenna M.C., Stevenson J.H., Huang X., Hopkins I.B., 2000. Differential distribution of the enzymes glutamate dehydrogenase and aspartate aminotransferase in cortical synaptic mitochondria contributes to metabolic compartmentation in cortical synaptic terminals. *Neurochem. Int.* 37, 229–241, [https://doi.org/10.1016/S0197-0186\(00\)00042-5](https://doi.org/10.1016/S0197-0186(00)00042-5)
- Murray A.J., Montgomery H.E., Feelisch M., Grocott M.P.W., Martin D.S., 2018. Metabolic adjustment to high-altitude hypoxia: from genetic signals to physiological implications. *Biochem. Soc. Trans.* 46, 599–607, <https://doi.org/10.1042/BST20170502>
- Nassereddine S., Habbal R., Kassouge Y., Kaltoum A.B.O., Farah K., Majda H., Rhizlane A.E., Nadifi S., Dehbi H., 2021. Analysis of the influence of glutathione S-transferase (*GSTM1* and *GSTT1*) genes on the risk of essential hypertension. *Ann. Hum. Biol.* 48, 585–589, <https://doi.org/10.1080/03014460.2022.2039291>
- Nemkov T., Sun K., Reisz J.A., Song A. et al., 2018. Hypoxia modulates the purine salvage pathway and decreases red blood cell and supernatant levels of hypoxanthine during refrigerated storage. *Haematologica* 103, 361–372, <https://doi.org/10.3324/haematol.2017.178608>
- Pan S., Zhang T., Rong Z. et al., 2017. Population transcriptomes reveal synergistic responses of DNA polymorphism and RNA expression to extreme environments on the Qinghai-Tibetan Plateau in a predatory bird. *Mol. Ecol.* 26, 2993–3010, <https://doi.org/10.1111/mec.14090>
- Pankaj K., Sugadev R., Sarkar S., Singh S.B., 2016. A network-based analysis of proteins involved in hypoxia stress and identification of leader proteins. *J. Proteomics Enzymol.* 5, <https://doi.org/10.4172/2470-1289.1000126>
- Peng X., Dai Z., Wang X., 2020. Comparative proteomic analysis to probe into the differences in protein expression profiles and toxicity bases of *Latrodectus tredecimguttatus* spiderlings and adult spiders. *Comp. Biochem. Physiol. C Toxicol. Pharmacol.* 232, 108762, <https://doi.org/10.1016/j.cbpc.2020.108762>
- Provost E., Weier C.A., Leach S.D., 2013. Multiple ribosomal proteins are expressed at high levels in developing zebrafish endoderm and are required for normal exocrine pancreas development. *Zebrafish* 10, 161–169, <https://doi.org/10.1089/zeb.2013.0884>
- Qi L., Chen Y., Shi K., Ma H., Wei S., Sha Z., 2021. Combining of transcriptomic and proteomic data to mine immune-related genes and proteins in the liver of *Cynoglossus semilaevis* challenged with *Vibrio anguillarum*. *Comp. Biochem. Physiol. Part D Genomics Proteomics* 39, 100864, <https://doi.org/10.1016/j.cbd.2021.100864>
- Salju J.K., Bawa-Allah K.A., 2012. Toxicological effects of lead and zinc on the antioxidant enzyme activities of post juvenile *Claris gariepinus*. *Resour. Env. Res.* 2, 21–26, <https://doi.org/10.5923/j.re.20120201.03>
- Saxena V., Orgill D., Kohane I., 2007. A set of genes previously implicated in the hypoxia response might be an important modulator in the rat ear tissue response to mechanical stretch. *BMC Genomics* 8, 430, <https://doi.org/10.1186/1471-2164-8-430>
- Shah A.N., Cadinu D., Henke R.M., Xin X., Dastidar R.G., Zhang L., 2011. Deletion of a subgroup of ribosome-related genes minimizes hypoxia-induced changes and confers hypoxia tolerance. *Physiol. Genomics* 43, 855–872, <https://doi.org/10.1152/physiolgenomics.00232.2010>
- Shao Y., Wellman T.L., Lounsbury K.M., Zhao F.Q., 2014. Differential regulation of GLUT1 and GLUT8 expression by hypoxia in mammary epithelial cells. *Am. J. Physiol. Regul. Integr. Comp. Physiol.* 307, 237–247, <https://doi.org/10.1152/ajpregu.00093.2014>
- Sharma N.K., Sethy N.K., Bhargava K., 2013. Comparative proteome analysis reveals differential regulation of glycolytic and antioxidant enzymes in cortex and hippocampus exposed to short-term hypobaric hypoxia. *J. Proteomics* 79, 277–298, <https://doi.org/10.1016/j.jprot.2012.12.020>
- Tran Q., Lee H., Park J., Kim S.H., Park J., 2016. Targeting cancer metabolism-revisiting the Warburg effects. *Toxicol. Res.* 32, 177–193, <https://doi.org/10.5487/TR.2016.32.3.177>
- Usman M., Zhao S., Jeon B.H., Salama E.S., Li X., 2022. Microbial β-oxidation of synthetic long-chain fatty acids to improve lipid biomethanation. *Water Res.* 213, 118164, <https://doi.org/10.1016/j.watres.2022.118164>
- Velasco-Martínez I.C., Hernández-Camacho C.J., Méndez-Rodríguez L.C., Zenteno-Savín T., 2016. Purine metabolism in response to hypoxic conditions associated with breath-hold diving and exercise in erythrocytes and plasma from bottlenose dolphins (*Tursiops truncatus*). *Phys. A Mol. Integr. Physiol.* 191, 196–201, <https://doi.org/10.1016/j.cbpa.2015.10.021>
- Wang Y.Y., Zhou Y., Fu H.C., Huang H.Z., Li N.Q., Jin R.M., Fu X.Z., Li N.Q., 2021. Transcriptomic and proteomic analyses of the immune mechanism in pathogenetic and resistant mandarin fish (*Sniperca chuatsi*) infected with ISKNV. *Aquaculture* 545, 737198, <https://doi.org/10.1016/j.aquaculture.2021.737198>
- Whiffen L.K., Midgley D.J., McGee P.A., 2007. Polyphenolic compounds interfere with quantification of protein in soil extracts using the Bradford method. *Soil Biol. Biochem.* 39, 691–694, <https://doi.org/10.1016/j.soilbio.2006.08.012>
- Wiśniewski J., Zougman A., Nagaraj N., Mann M., 2009. Universal sample preparation method for proteome analysis. *Nat. Methods* 6, 359–362, <https://doi.org/10.1038/nmeth.1322>
- Wong Y.H., Zhang Y., Lun J., Qiu J.W., 2021. A proteomic analysis of skeletal tissue anomaly in the brain coral *Platygyra carnosa*. *Mar. Pollut. Bull.* 164, 111982, <https://doi.org/10.1016/j.marpolbul.2021.111982>

- Xiao S.J., Mou Z.B., Yang R.B., Fan D.D., Liu J.Q., Zou Y., Zhu S.L., Zou M., Zhou C.W., Liu H.P., 2021. Genome and population evolution and environmental adaptation of *Glyptosternon maculatum* on the Qinghai-Tibet Plateau. *Zool. Res.* 42, 502–513, <https://doi.org/10.24272/j.issn.2095-8137.2021.096>
- Yang W., Liu J., Hou L., Chen Q., Liu Y., 2021. Shikonin differentially regulates glucose metabolism via PKM2 and HIF1 $\alpha$  to overcome apoptosis in a refractory HCC cell line. *Life Sci.* 265, 118796, <https://doi.org/10.1016/j.lfs.2020.118796>
- Yoon J., Kim Y.H., Min J., 2017. Evaluation of *in vitro* function by sub-cellular distribution of lysosomal and peroxisomal protein in *Saccharomyces cerevisiae*. *J. Nanosci. Nanotechnol.* 17, 244–250, <https://doi.org/10.1166/jnn.2017.12448>
- Yu M., He S., 2012. Phylogenetic relationships and estimation of divergence times among *Sisoridae catfishes*. *Sci. China Life Sci.* 55, 312–320, <https://doi.org/10.1007/s11427-012-4305-z>
- Zera K., Sweet R., Zastre J., 2016. Role of HIF-1 $\alpha$  in the hypoxia inducible expression of the thiamine transporter, *SLC19A3*. *Gene* 595, 212–220, <https://doi.org/10.1016/j.gene.2016.10.013>
- Zera K., Zastre J., 2017. Thiamine deficiency activates hypoxia inducible factor-1 $\alpha$  to facilitate pro-apoptotic responses in mouse primary astrocytes. *PLoS ONE* 12, e0186707, <https://doi.org/10.1371/journal.pone.0186707>
- Zhang G.Q., Mou Z., Xue W.H., Liu H., 2021. Phosphorylated protein modification analysis on normal liver and exo-celiac liver of *Glyptosternon maculatum*. *J. Fish Biol.* 99, 1696–1707, <https://doi.org/10.1111/jfb.14877>
- Zhang H., Zhang W., Huang S., Xu P., Cao Z., Chen M., Lin X., 2022. The potential role of plasma membrane proteins in response to Zn stress in rice roots based on iTRAQ and PRM under low Cd condition. *J. Hazard. Mater.* 429, 128324, <https://doi.org/10.1016/j.jhazmat.2022.128324>
- Zhou X., Zhou L., Ge X., Guo X., Han J., Zhang Y., Yang H., 2020. Quantitative proteomic analysis of porcine intestinal epithelial cells infected with porcine deltacoronavirus using iTRAQ-Coupled LC-MS/MS. *J. Proteome Res.* 19, 4470–4485, <https://doi.org/10.1021/acs.jproteome.0c00592>